ARTICLE

doi:10.1038/nature18611

A novel cereblon modulator recruits GSPT1 to the CRL4^{CRBN} ubiquitin ligase

Mary E. Matyskiela[1]*, Gang Lu[1]*, Takumi Ito[2]*, Barbra Pagarigan[1], Chin-Chun Lu[1], Karen Miller[1], Wei Fang[1], Nai-Yu Wang[1], Derek Nguyen[1], Jack Houston[1], Gilles Carmel[1], Tam Tran[1], Mariko Riley[1], Lyn'Al Nosaka[3], Gabriel C. Lander[3], Svetlana Gaidarova[1], Shuichan Xu[1], Alexander L. Ruchelman[1], Hiroshi Handa[2], James Carmichael[1], Thomas O. Daniel[1], Brian E. Cathers[1], Antonia Lopez-Girona[1] & Philip P. Chamberlain[1]

Immunomodulatory drugs bind to cereblon (CRBN) to confer differentiated substrate specificity on the CRL4^{CRBN} E3 ubiquitin ligase. Here we report the identification of a new cereblon modulator, CC-885, with potent anti-tumour activity. The anti-tumour activity of CC-885 is mediated through the cereblon-dependent ubiquitination and degradation of the translation termination factor GSPT1. Patient-derived acute myeloid leukaemia tumour cells exhibit high sensitivity to CC-885, indicating the clinical potential of this mechanism. Crystallographic studies of the CRBN–DDB1–CC-885–GSPT1 complex reveal that GSPT1 binds to cereblon through a surface turn containing a glycine residue at a key position, interacting with both CC-885 and a 'hotspot' on the cereblon surface. Although GSPT1 possesses no obvious structural, sequence or functional homology to previously known cereblon substrates, mutational analysis and modelling indicate that the cereblon substrate Ikaros uses a similar structural feature to bind cereblon, suggesting a common motif for substrate recruitment. These findings define a structural degron underlying cereblon 'neosubstrate' selectivity, and identify an anti-tumour target rendered druggable by cereblon modulation.

The immunomodulatory drugs lenalidomide and pomalidomide promote recruitment and ubiquitination of substrate proteins to the CRL4^{CRBN} (CUL4–DDB1–RBX1–CRBN) E3 ubiquitin ligase, leading to their subsequent degradation by the 26S proteasome[1,15,16]. The therapeutic benefits of immunomodulatory drug treatment in multiple myeloma and 5q-deletion-associated myelodysplastic syndrome are driven by a combination of both anti-proliferative cellular and immunomodulatory effects[2–5]. The CRL4^{CRBN} E3 ubiquitin ligase complex consists of a core scaffolding component CUL4, which binds to the RBX1 subunit, the docking site for E2 recruitment, and DDB1, an adaptor protein. DDB1 provides a binding site for CRL4 substrate receptor proteins such as cereblon, termed DCAFs (DDB1 and CUL4 associated factors), which recruit substrates to the ubiquitin ligase complex and determine substrate specificity[6–9].

Structural studies have shown that immunomodulatory drugs bind in a shallow hydrophobic pocket on the surface of cereblon[10,11]. Cereblon binding is mediated by a glutarimide ring, a feature common to the clinical molecules thalidomide, lenalidomide, pomalidomide, and CC-122. These compounds feature additional chemical groups that are not contained by the cereblon binding pocket, and have been postulated to interact with cognate substrates resulting in 'neomorphic' E3 ligase activity. Several proteins have been reported to be ubiquitinated by the CRL4^{CRBN} E3 ligase upon treatment with immunomodulatory drugs. Ikaros and Aiolos are zinc finger transcription factors important in haematological differentiation[12,13], which are degraded by addition of several immunomodulatory drugs[5,14–16]. Recently, lenalidomide, but not pomalidomide or CC-122, was demonstrated to induce the degradation of the protein kinase casein kinase 1α (CK1α), thereby exploiting CK1α haploinsufficiency associated with 5q-deletion-associated myelodysplastic syndrome[5]. Importantly, these cereblon substrates share no obvious sequence or structural homology to explain their susceptibility to immunomodulatory drugs.

We investigated whether cereblon could be repurposed to induce the degradation of previously unidentified targets resulting in anti-tumour activity. We identified CC-885 as a potent anti-cancer agent eliciting broad spectrum growth inhibition against cancer cell lines and patient-derived acute myeloid leukaemia (AML) cells, indicating the clinical potential for this mechanism. We identified GSPT1 (eRF3a) as a novel CC-885-dependent cereblon substrate mediating the anti-proliferative effects of CC-885. GSPT1 is a translation termination factor that binds eRF1 to mediate stop codon recognition and nascent protein release from the ribosome[17–19]. GSPT1 is not targeted for degradation by any of the current generation of clinically approved immunomodulatory drugs, and possesses no obvious homology to Ikaros, Aiolos or CK1α. To investigate the structural determinants for substrate recruitment, we solved the structure of cereblon in complex with DDB1, CC-885, and GSPT1. We found that the main contacts to cereblon–CC-885 by GSPT1 are mediated by the peptide backbone of a surface turn. Degrons, molecular motifs that direct E3 ligase interactions, have been defined for other ligases[20–22], and include examples where recognition is dependent upon small molecules binding to the ligase complex[23,24]. Mutational evidence indicates that Ikaros is recruited via a motif similar to that of GSPT1, demonstrating that there is a common structural degron for ligand-directed recruitment to the CRL4^{CRBN} E3 ligase.

CC-885 is a cereblon-dependent anti-tumour agent

On the basis of the hypothesis that additional proteins are vulnerable to cereblon-mediated degradation, we sought to identify cereblon ligands with unique activities from a library of analogues. CC-885 was identified as a compound exhibiting a strong anti-proliferative phenotype in tumour cell lines (Extended Data Fig. 1a). The broad activity profile of CC-885 is highly differentiated from that of thalidomide, lenalidomide and pomalidomide (Extended Data Fig. 1a, d). To assess the potential

[1]Celgene Corporation, 10300 Campus Point Drive, Suite 100, San Diego, California 92121, USA. [2]Department of Nanoparticle Translational Research, Tokyo Medical University, Shinjuku-ku, Tokyo 160-8402, Japan. [3]The Scripps Research Institute, San Diego, California 92121, USA.
*These authors contributed equally to this work.

clinical utility of CC-885, the molecule was tested in an *ex vivo* setting to evaluate potency against patient-derived AML tumour cells. CC-885 exhibited sub-nanomolar potency against 4 out of 5 patient samples (Extended Data Fig. 1b), with reduced activity against the normal lymphoid cells obtained from the same donors.

We next established the cellular target of CC-885. Like lenalidomide and its analogues, CC-885 contains a glutarimide ring that can directly interact with cereblon (Fig. 1a). The anti-proliferative effects of CC-885 are cereblon-dependent, as ablation of cereblon gene expression using clustered regularly interspaced short palindromic repeats (CRISPR) conferred resistance to CC-885 in 293FT human embryonic kidney cells, as well as in the AML cell lines NB-4, MOLM-13 and OCI-AML2 (Fig. 1 b, Extended Data Fig. 1c). To identify potential substrates of $CRL4^{CRBN}$ regulated by CC-885, we generated 293T HEK cells stably expressing Flag- and haemagglutinin (HA)-double-tagged cereblon (FH–CRBN). Using large-scale anti-Flag affinity purification followed by mass spectrometry analysis, GSPT1 (eRF3a) was identified as a protein that associated with FH–CRBN specifically in the presence of CC-885 (Fig. 1c, Supplementary Information Table 1). The presence of GSPT1 in the anti-Flag immunoprecipitates of FH–CRBN complex bound to CC-885 was confirmed by immunoblot analysis (Fig. 1c, bottom). Reciprocal binding assays performed with HA-tagged GSPT1 immobilized on anti-HA resin further supported that CC-885 could enhance the binding affinity of endogenous cereblon for GSPT1 (Extended data Fig. 2). Lenalidomide did not promote the interactions between cereblon and GSPT1. Conversely, CC-885 enhanced the binding of Ikaros (IKZF1) to cereblon. Consistent with the binding data, CC-885, but not lenalidomide or pomalidomide, triggered the depletion of GSPT1, whereas all three agents decreased the level of Ikaros in NB-4 leukaemia cells (Fig. 1d).

CC–885 promotes cereblon–dependent GSPT1 destruction

We next determined whether the changes in GSPT1 protein levels upon CC-885 treatment resulted from $CRL4^{CRBN}$-dependent ubiquitination and degradation. In 293FT HEK cells, the CC-885-induced reduction of GSPT1 protein levels can be prevented by depletion of cereblon via CRISPR or by co-treatment with either a neddylation inhibitor (MLN4924) or a proteasome inhibitor (MG132) (Extended Data Fig. 3, and data not shown). The mRNA level of GSPT1 was not decreased but rather increased in 293FT HEK cells treated with CC-885, consistent with a non-transcriptional mechanism (Extended Data Fig. 3). Together, these results indicate that CC-885 treatment causes cereblon-dependent ubiquitination and subsequent proteosomal degradation of GSPT1.

CC-885 promoted both the *in vivo* and *in vitro* ubiquitination of GSPT1 by cereblon (Fig. 1 e, f and Extended Data Fig. 4) and decreased the protein half-life of GSPT1 in 293FT HEK parental but not in $CRBN^{-/-}$ cells (Extended Data Fig. 4). Reintroduction of wild-type cereblon via lentiviral infection in 293FT $CRBN^{-/-}$ cells restored the CC-885-dependent degradation of GSPT1, whereas CRBN(W386A) and CRBN(E377V) mutants displayed diminished activity, with E377V exhibiting a stronger effect consistent with the critical role of E377 in anchoring CC-885 in the cereblon–GSPT1 complex (Extended Data Fig. 4).

GSPT1 depletion drives CC–885 effects

To address whether the cereblon-dependent degradation of GSPT1 was responsible for the cytotoxic effects of CC-885, a GSPT1 mutant that retains its normal function, but loses CC-885-dependent cereblon binding, was used to distinguish the role of GSPT1 from that of other substrates. The yeast homologue, SUP35, shares a high degree of

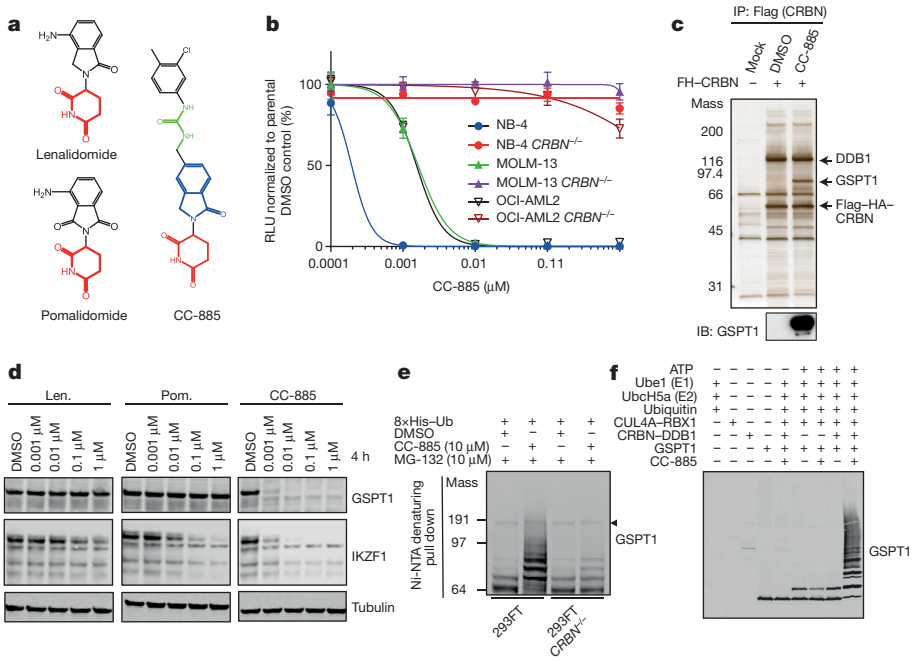

Figure 1 | GSPT1 is a substrate of the cereblon E3 ligase complex bound with CC-885. a, Structures of lenalidomide, pomalidomide and CC-885 with the glutarimide ring shown in red, isoindolinone in blue, the methylene urea in green. **b**, The effect of CC-885 on cell proliferation in parental and $CRBN^{-/-}$ AML cell lines as indicated. Result is representative of three biological replicates. Data are shown as mean ± s.d., $n = 3$ technical replicates. **c**, Silver stained gel of the immunoprecipitation of Flag-tagged cereblon to identify GSPT1 binding in the presence of CC-885. **d**, Immunoblot analysis of whole-cell extracts of NB-4 cells incubated with DMSO, or with lenalidomide, pomalidomide or CC-885 at the concentrations indicated for 4 h. **e**, The *in vivo* ubiquitination of GSPT1 is cereblon dependent. 293FT $CRBN^{-/-}$ cells were transfected with plasmids expressing 8× His–Ub. After 48 h, cells were treated with CC-885 and MG-132 as indicated for 8 h. Whole–cell extract and ubiquitinated protein products enriched with nickel sepharose were subjected to immunoblot analysis. The anti-His ubiquitin immunoblot showing equal enrichment of ubiquitinated proteins is shown in Extended Data Fig. 3a. Arrowhead indicates nonspecific band. **f**, *In vitro* ubiquitination of GSPT1 by the CUL4A–RBX1–DDB1–cereblon complex. Recombinant protein products as indicated were incubated with or without ATP (10 mM) and CC-885 (100 μM) in the ubiquitination assay buffer at 30 °C for 2 h, and then analysed by immunoblotting. Results in **d**–**f** are representative of three independent experiments. For gel source data, see Supplementary Information Fig. 1.

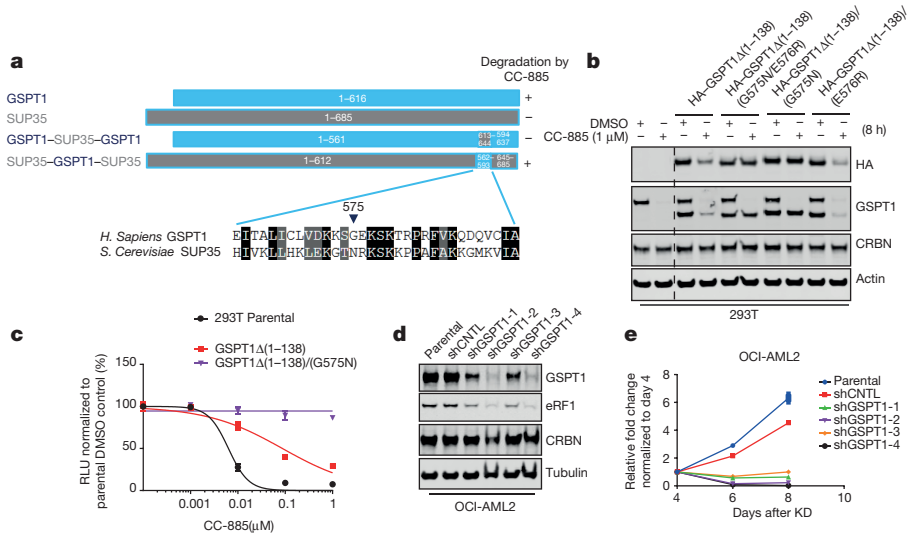

Figure 2 | GSPT1 degradation is necessary and sufficient for the CC-885-associated cytotoxicity. a, Schematic of the human GSPT1 and *Saccharomyces cerevisiae* SUP35 chimaeras. The CC-885-dependent degradation motif of human GSPT1, as well as the corresponding region present in SUP35, are highlighted. Change of protein stability of the GSPT1–SUP35 fusion proteins in response to CC-885 treatment is shown in Extended Data Fig. 5d. **b**, Immunoblot analysis of 293T HEK cells stably producing HA-tagged GSPT1 wild-type and variants. Dotted line marks where irrelevant lanes were removed. Detailed domain mapping experiments are shown in Extended Data Fig. 5. **c**, Effect of CC-885 on proliferation of 293T parental cells or stably expressing GSPT1 variants. Result is representative of three biological replicates. Data are presented as mean ± s.d., $n = 3$ technical replicates. **d**, **e**, Cell growth curve of OCI-AML2 parental cells or cells transduced with lentiviral vectors expressing a control shRNA (shCNTL) or GSPT1 specific shRNA (shGSPT1-1 to 4). Immunoblot analysis of whole-cell extracts (**d**) was carried out at day 4 after transduction with lentiviral vectors. Cell growth (**e**) was quantified with CellTiter-Glo (CTG) at day 4, 6, and 8 after transduction. Results are representative of three biological replicates. Data are mean ± s.d. $n = 3$ technical replicates. For gel source data, see Supplementary Information Fig. 1.

sequence homology with human GSPT1, but did not show any changes in protein level in response to CC-885 when stably expressed in 293T HEK cells (Extended Data Fig. 5). Through a series of domain-swap experiments, we identified that conversion of GSPT1 glycine 575 into the corresponding asparagine of SUP35 prevented both the CC-885-induced degradation of GSPT1 and the *in vitro* binding to cereblon (Fig. 2a, Extended Data Fig. 5). We then tested CC-885 in 293T HEK cells stably expressing the CC-885-sensitive or -resistant GSPT1 variants. Overexpression of a resistant variant GSPT1Δ(1–138)/(G575N) completely abrogated the CC-885-induced anti-proliferation (Fig. 2b, c), whereas overexpression of a CC-885-sensitive variant GSPT1Δ(1–138) only conferred partial protection. Similar results were obtained in AML cell lines OCI-AML2 and MOLM-13 (Extended Data Fig. 6a, b). To determine whether GSPT1 depletion is sufficient to block cell proliferation, we used lentiviral short hairpin RNA (shRNA) vectors to silence the expression of endogenous GSPT1 in 293T HEK, OCI-AML2, and MOLM-13 cells and found a marked reduction of GPST1 protein level correlated with decreased cell fitness as compared to parental cells or cells expressing a control shRNA (Fig. 2d, e and Extended Data Fig. 6c–e). Together, these experiments indicate that CC-885 cytotoxicity largely, if not completely, depends upon loss of GSPT1. This is consistent with a previously published report showing that mutation of *SUP35* prevented the G1 to S phase transition during cell cycle progression in *Saccharomyces cerevisiae*[25]. Similarly, depletion of GSPT1 led to cell cycle arrest at G1 in the human colorectal cancer cell line HCT116 (ref. 26).

Structure of cereblon with DDB1, CC-885 and GSPT1

To explore the molecular requirements for ligand-directed substrate recruitment to cereblon, we determined the crystal structure of full-length human DDB1 bound to human cereblon (amino acids 40–442), CC-885, and domains 2 and 3 of human GSPT1 (amino acids 437–633) to 3.6 Å resolution (Fig. 3a, full data collection and refinement statistics given in Extended Data Table 1). In the crystal structure, GSPT1 domain 3 docks against cereblon at the site of CC-885 binding with direct interactions with both CC-885 and the proximal cereblon surface (Fig. 3a). GSPT1 domain 2 does not directly contact either CC-885 or cereblon. Cereblon is bound to DDB1 in a manner consistent with the previously determined structures of cereblon–DDB1 (refs 10, 11). CC-885 is bound in the tri-Trp pocket of cereblon, where the glutarimide ring makes 3 hydrogen bonds with cereblon, two to the backbone of residues W380 and H378, and one to the side chain of H378 (Fig. 3b). The isoindolinone ring of CC-885 (Fig. 1a) is presented on the surface of cereblon in a manner similar to lenalidomide, and interacts with both cereblon and GSPT1, including a hydrogen bond from the isoindolinone carbonyl oxygen to the side chain of N351 of cereblon. The chemical structure of CC-885 is extended compared to lenalidomide or pomalidomide (Fig. 1a), allowing further interactions with both cereblon and GSPT1. The urea moiety of CC-885 is positioned between cereblon residues E377 and H353, with hydrogen bonds to both side chains. The terminal methyl-chloro-phenyl ring is positioned proximal to the β-sheet core of GSPT1 domain 3.

CC-885 is critical for the formation of the complex as demonstrated by surface plasmon resonance experiments showing that GSPT1 binds to cereblon-DDB1 with a dissociation constant (K_D) of ~350 nM in the presence of CC-885 (Extended Data Fig. 7). No significant interaction was observed in the absence of CC-885. Similarly, negative stain electron microscopy confirmed that CC-885 was critical for cereblon–GSPT1 complex formation, as no cereblon–GSPT1 particles were observed in the absence of CC-885 (Extended Data Fig. 8).

GSPT1 binds a 'hotspot' on the cereblon–CC-885 surface

It was previously hypothesized that immunomodulatory drug binding forms an interaction hotspot on the cereblon surface by placement of a planar hydrophobic group (the ligand phthalimide or isoindolinone ring, Fig. 1a) amongst unsatisfied hydrogen bonds from both ligand and the protein surface[10]. In this way, ligands with low molecular weight would be able to achieve marked alterations in binding potency by promoting contributions towards substrate binding from the cereblon surface. The structure of cereblon–DDB1–CC-885–GSPT1 confirms that GSPT1 interacts directly with CC-885 and also forms

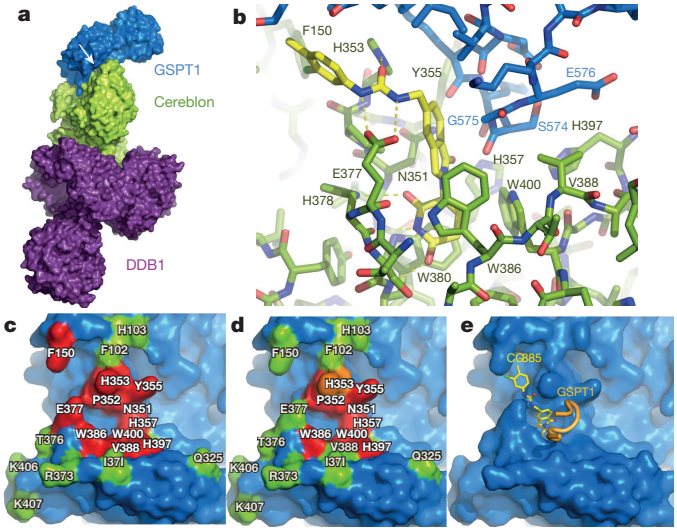

Figure 3 | Crystal structure of the cereblon–DDB1–GSPT1–CC-885 complex. a, Surface representation with DDB1 shown in purple, cereblon in green and GSPT1 in blue. Position of CC-885 is indicated by an arrow. **b**, Details of the interface between cereblon and GSPT1 with CC-885 shown as sticks with carbons in yellow. Hydrogen bonds between CC-885 and cereblon are shown as yellow dotted lines. **c**–**e**, The effect of cereblon surface mutagenesis on substrate binding (see also Extended Data Fig. 9). Red indicates a strong reduction in substrate binding following mutation to alanine, orange indicates some reduction, and green indicates no effect. Blue surface areas were not tested. **c**, The effect of the mutations on GSPT1 recruitment; **d**, the mutational results for Ikaros binding; **e**, the relative positions of CC-885 (yellow sticks) and the GSPT1 cereblon-interacting motif (orange).

direct protein–protein interactions, with cereblon residues N351, H357, and W400 all contributing direct hydrogen bonds to GSPT1. Further van der Waals interactions are provided from the side chains of cereblon residues Y355, H397, and V388.

Co-immunoprecipitation of GSPT1 with cereblon surface mutants reveals that residues including N351, H357, E377, V388 and H397 are critical to recruiting GSPT1 to cereblon in a manner dependent upon CC-885 (Fig. 3c, Extended Data Fig. 9). Each of the three side chains that hydrogen bond to GSPT1 (N351, H357 and W400) is shown to be critical for GSPT1 recruitment. When mutation sensitivity is mapped onto the surface of cereblon by colour, a patch of sensitivity is revealed that corresponds to the interaction site visible in the crystal structure (Fig. 3c, e).

To evaluate whether this patch of the cereblon surface is similarly purposed for the recruitment of other substrates, the same panel of cereblon mutants was tested against Ikaros (Fig. 3d, Extended Data Fig. 9). As shown in Fig. 3c, d, the critical interaction site is similar between GSPT1 and Ikaros. Interestingly, all three residues that contribute hydrogen bonds to GSPT1 are also required for Ikaros recruitment, suggesting a common mechanism of substrate recruitment. Residues E377 and F150, however, are uniquely required for GSPT1 recruitment. F150 is proximal to CC-885 and contacts domain 3 of GSPT1 in a manner that is dependent on the GSPT1 tertiary structure; it is therefore probably different from other substrates that do not share a common fold. E377 makes direct interactions with CC-885, and mutation may therefore affect ligand binding and conformation. An E377V polymorphism is found in mouse and rats and underlies resistance to CC-885 treatment in rodents (Extended Data Fig. 9 e and Supplementary Discussion). A further difference in cereblon–substrate interactions is observed at V388: GSPT1 binding is lost in the V388A mutant, but some binding is retained in the V388I mutant, which is also a rodent polymorphism. In contrast, Ikaros binding is abolished by the V388I mutation, consistent with previous work[5]; however, the V388A mutation has no significant effect on Ikaros binding. These differences may be due to subtle differences in residue side chain bulk or substrate conformation at the interaction site. Lenalidomide and pomalidomide do not cause GSPT1 binding and degradation (Fig. 1b and Extended Data Fig. 2). These molecules lack the urea and chloro-methyl-phenyl moieties of CC-885 (Fig. 1a) that probably contribute to the affinity of the complex through interactions with domain 3 of GSPT1.

GSPT1 features required for recruitment to cereblon

The GSPT1 motif that mediates interactions with cereblon–CC-885 is a solvent-exposed region composed of residues 569–578, including a small anti-parallel β-sheet forming a β-hairpin with an α-turn from residues 571–575 (Fig. 4a). Despite the degree of solvent exposure, the turn is well-ordered in both the previous GSPT1 crystal structure[17] and in the complex with cereblon. The conformational stability of the turn is probably due to intramolecular bonding, with an ASX-motif and an ST-turn mediated by D571 and S574, respectively. These intramolecular motifs might be expected to rigidify and stabilize the conformation of the turn before cereblon binding (Fig. 4a). The key hydrogen bonds formed with cereblon are all mediated by backbone carbonyl oxygen atoms, which are displayed in an array at the end of the turn. Carbonyl oxygen atoms from GSPT1 K572, K573, and S574 accept hydrogen bonds from cereblon residues N351, H357, and W400, respectively (Fig. 4a). The GSPT1 turn lies on top of the isoindolinone ring of CC-885 making hydrophobic and van der Waals interactions. A further key interaction occurs between G575 and the isoindolinone moiety. G575 is of particular importance in determining substrate recruitment, as it not only contributes to binding interactions, but also the close sterics at this position indicate that no other residue would be tolerated at this position. Therefore, the degron is not the linear peptide sequence, but rather the geometric arrangement of three backbone hydrogen bond acceptors at the apex of a turn (positions i, i+1, and i+2), with a glycine residue at a key position (i+3).

The structural interpretation is supported by site-directed mutagenesis of the GSPT1 turn, which indicates that G575A loses CC-885-dependent cereblon binding (Fig. 4c). It should be noted that the backbone torsion angles of G575 occupy a part of the Ramachandran plot only accessible to glycine residues and mutagenesis may alter both side chain decoration and backbone position. V570 exhibits van der Waals interactions with the methylene–urea linker, and accordingly, the V570A mutant displays reduced cereblon binding (Fig. 4a, c). Consistent with their expected role in stabilizing the turn conformation, both D571A and S574A mutants lose cereblon binding (Fig. 4c). However, the side chains of residues K572, K573 and E576 do not affect GSPT1 binding to cereblon, consistent with the crystal structure that indicates these residues have minimal side chain interactions with cereblon. The fact that key bonds are formed from the peptide backbone of GSPT1, rather than from side chain residues, presents the intriguing possibility that there may be considerable sequence tolerance in substrate recruitment, as long as the backbone remains in the appropriate conformation.

Ikaros binds via a similar structural motif

GSPT1 contains no obvious structural or sequence homology to the previously identified cereblon substrates such as the protein kinase CK1α or the zinc finger transcription factor Ikaros. However, the similar pattern of sensitivity to mutations on the surface of cereblon (Fig. 3c, d) suggests that a similar anchoring motif may be present in Ikaros. On the basis of the observation that the GSPT1 interactions with cereblon were mediated by the protein backbone, we constructed a homology model of Ikaros and examined this for a similar surface turn. The homology model of Ikaros indicated that a zinc finger domain is indeed capable of presenting a turn that can make the three key hydrogen bonds with a glycine residue at the critical position on the solvent-accessible surface of the domain (Fig. 4b). Consistent with this prediction, a minimal domain of Ikaros containing only this single predicted zinc finger domain (amino acids 140–168),

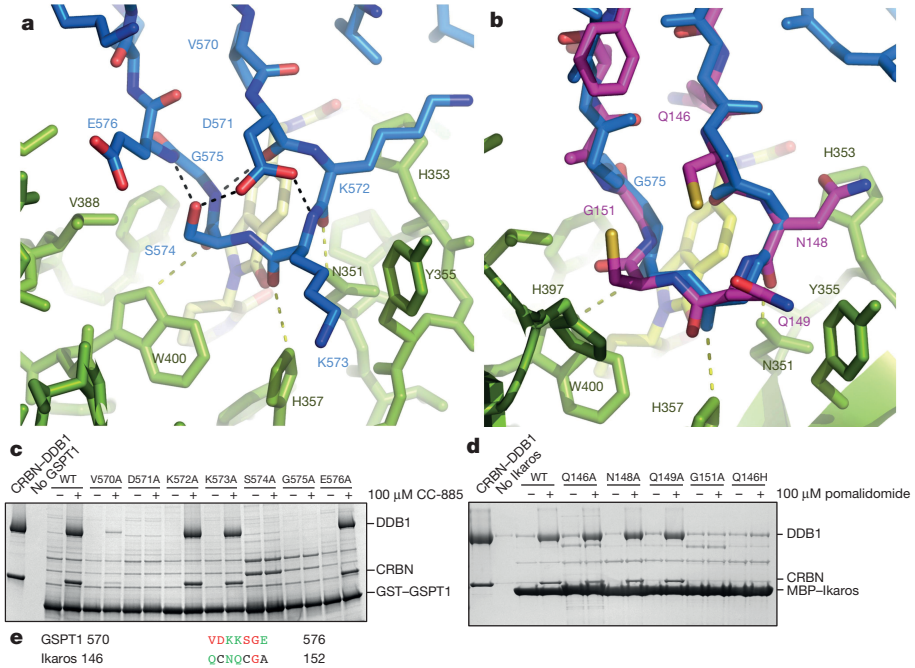

Figure 4 | Substrate proteins bind cereblon via a surface turn. a, The anchoring motif of GSPT1 (blue) bound to cereblon (green) and CC-885 (yellow). **b**, A model of Ikaros (magenta) superimposed onto the backbone of GSPT1 (blue). **c**, Coomassie-stained gels of cereblon–DDB1 pull-down by GST–GSPT1 (amino acids 526–633), with alanine mutations of the GSPT1 anchoring motif. **d**, Cereblon–DDB1pull-down with MBP–Ikaros (amino acids 140–168) with alanine mutations of the proposed Ikaros anchoring motif. This experiment is representative of three independent replicates (**c**, **d**). **e**, Sequence alignment of the GSPT1-anchoring motif with the putative region from Ikaros, with residues shown to be critical for binding in red, and those where an alanine mutation was tolerated in green. The critical glycine residue is shown in bold. Ikaros C147 and C150 were not mutated as they coordinate a structural zinc ion (not shown). For gel source data, see Supplementary Information Fig. 1.

is sufficient to pull down cereblon–DDB1 in the presence of pomalidomide (Fig. 4d).

Crucially, there is no sequence homology between Ikaros and GSPT1 in the anchoring motif regions as modelled, except for the glycine residue at position i+3 (Fig. 4e). The implications of this model were tested by co-immunoprecipitation of cereblon with mutations targeting each residue of the putative Ikaros anchoring motif. Mutation of the key glycine residue (G151) to alanine disrupts cereblon interactions (Fig. 4d). It was previously demonstrated that the Q146H mutation causes a reduction of cereblon binding[15,16]. The putative anchoring motif modelled in Ikaros positions the critical residue, Q146, in a position oriented towards both bound ligand and the cereblon surface. Mutation of the putative anchoring motif in Ikaros confirms that Q146H causes a reduction in cereblon binding (Fig. 4d, Extended Data Fig. 2a). In contrast, the Q146A mutation is similar to wild type, suggesting that steric or electronic hindrance of a histidine residue at this position, rather than loss of key interactions from the glutamine, is responsible for the loss of cereblon binding in the Q146H mutants. N148A and Q149A mutations in the proposed anchoring motif of Ikaros do not affect cereblon binding, in a manner analogous to the equivalent positions K572 and K573 in GSPT1 (Fig. 4 c, d). C147 and C150 are responsible for coordination of a structural zinc ion, and were therefore not examined by mutagenesis out of concern for disruption of the zinc finger domain structure. Structural studies on Ikaros family members in complex with cereblon will be necessary to identify the full atomic details of the interactions.

Discussion

In this work, we have extended the clinical scope of cereblon-modulating activities with the identification of a novel ligand, CC-885, which is potently anti-proliferative in cancer cell lines. CC-885 directs cereblon to target GSPT1, a substrate that is unrelated in fold and function to previously described substrates. Targeting of GSPT1 provides expanded clinical potential for cereblon modulators, with potent effects seen in both AML cell lines and in patient-derived tumour cells. Furthermore, by targeting what may have been considered an otherwise undruggable protein, the utility of directing cereblon for targeting diverse protein substrates posits a wide range of new therapeutic opportunities.

In contrast to linker-based approaches exploiting cereblon[27–29], CC-885 creates an interaction hotspot on the cereblon surface for direct protein–protein interactions with the substrate, underlying the gain-of-function 'chemo-neomorphic' activity. Although this may constrain the potential substrate range, the contribution from the cereblon surface supports the function of small drug-like molecules without the pharmacokinetic challenges that may accompany ligase modulators incorporating large flexible linkers.

Our structural work shows that cereblon recruits GSPT1 through the CC-885-induced recognition of a surface turn. A key to the steric compatibility is the presence of a glycine at the precise position within the turn. Significantly, except the glycine residue, the interactions are composed of hydrogen bonds from the backbone of GSPT1, indicating that the degron in this instance will not be revealed by primary sequence, but instead by the geometry and sterics. Our mutational and modelling work on Ikaros raises the intriguing possibility of a common structural degron occurring amongst diverse substrate proteins. Furthermore, after submission of this manuscript, a crystal structure of cereblon in complex with lenalidomide and CK1α was published that exhibits a binding mode consistent with our degron[30]. It may therefore be possible to rationally identify candidate neosubstrates by searching for the cereblon response element across the proteome. Such candidate substrates may then form targets for exploitation by the next generation of cereblon modulators.

Online Content Methods, along with any additional Extended Data display items and Source Data, are available in the online version of the paper; references unique to these sections appear only in the online paper.

Received 27 November 2015; accepted 31 May 2016.
Published online 22 June 2016.

1. Ito, T. *et al.* Identification of a primary target of thalidomide teratogenicity. *Science* **327,** 1345–1350 (2010).
2. Dimopoulos, M. A., Richardson, P. G., Moreau, P. & Anderson, K. C. Current treatment landscape for relapsed and/or refractory multiple myeloma. *Nat. Rev. Clin. Oncol.* **12,** 42–54 (2015).
3. Lopez-Girona, A. *et al.* Cereblon is a direct protein target for immunomodulatory and antiproliferative activities of lenalidomide and pomalidomide. *Leukemia* **26,** 2326–2335 (2012).
4. Zhu, Y. X. *et al.* Cereblon expression is required for the antimyeloma activity of lenalidomide and pomalidomide. *Blood* **118,** 4771–4779 (2011).
5. Krönke, J. *et al.* Lenalidomide induces ubiquitination and degradation of CK1α in del(5q) MDS. *Nature* **523,** 183–188 (2015).
6. Angers, S. *et al.* Molecular architecture and assembly of the DDB1–CUL4A ubiquitin ligase machinery. *Nature* **443,** 590–593 (2006).
7. Higa, L. A. *et al.* CUL4–DDB1 ubiquitin ligase interacts with multiple WD40-repeat proteins and regulates histone methylation. *Nat. Cell Biol.* **8,** 1277–1283 (2006).
8. Jin, J., Arias, E. E., Chen, J., Harper, J. W. & Walter, J. C. A family of diverse Cul4-Ddb1-interacting proteins includes Cdt2, which is required for S phase destruction of the replication factor Cdt1. *Mol. Cell* **23,** 709–721 (2006).
9. He, Y. J., McCall, C. M., Hu, J., Zeng, Y. & Xiong, Y. DDB1 functions as a linker to recruit receptor WD40 proteins to CUL4–ROC1 ubiquitin ligases. *Genes Dev.* **20,** 2949–2954 (2006).
10. Chamberlain, P. P. *et al.* Structure of the human Cereblon–DDB1–lenalidomide complex reveals basis for responsiveness to thalidomide analogs. *Nat. Struct. Mol. Biol.* **21,** 803–809 (2014).
11. Fischer, E. S. *et al.* Structure of the DDB1–CRBN E3 ubiquitin ligase in complex with thalidomide. *Nature* **512,** 49–53 (2014). 10.1038/nature13527.
12. John, L. B. & Ward, A. C. The Ikaros gene family: transcriptional regulators of hematopoiesis and immunity. *Mol. Immunol.* **48,** 1272–1278 (2011).
13. Dijon, M. *et al.* The role of Ikaros in human erythroid differentiation. *Blood* **111,** 1138–1146 (2008).
14. Gandhi, A. K. *et al.* Immunomodulatory agents lenalidomide and pomalidomide co-stimulate T cells by inducing degradation of T cell repressors Ikaros and Aiolos via modulation of the E3 ubiquitin ligase complex CRL4(CRBN.). *Br. J. Haematol.* **164,** 811–821 (2014).
15. Krönke, J. *et al.* Lenalidomide causes selective degradation of IKZF1 and IKZF3 in multiple myeloma cells. *Science* **343,** 301–305 (2014).
16. Lu, G. *et al.* The myeloma drug lenalidomide promotes the cereblon-dependent destruction of Ikaros proteins. *Science* **343,** 305–309 (2014).
17. Cheng, Z. *et al.* Structural insights into eRF3 and stop codon recognition by eRF1. *Genes Dev.* **23,** 1106–1118 (2009).
18. Preis, A. *et al.* Cryoelectron microscopic structures of eukaryotic translation termination complexes containing eRF1-eRF3 or eRF1-ABCE1. *Cell Reports* **8,** 59–65 (2014).
19. Zhouravleva, G. *et al.* Termination of translation in eukaryotes is governed by two interacting polypeptide chain release factors, eRF1 and eRF3. *EMBO J.* **14,** 4065–4072 (1995).
20. Hon, W. C. *et al.* Structural basis for the recognition of hydroxyproline in HIF-1 alpha by pVHL. *Nature* **417,** 975–978 (2002).
21. Min, J. H. *et al.* Structure of an HIF-1α-pVHL complex: hydroxyproline recognition in signaling. *Science* **296,** 1886–1889 (2002).
22. Glotzer, M., Murray, A. W. & Kirschner, M. W. Cyclin is degraded by the ubiquitin pathway. *Nature* **349,** 132–138 (1991).
23. Sheard, L. B. *et al.* Jasmonate perception by inositol-phosphate-potentiated COI1–JAZ co-receptor. *Nature* **468,** 400–405 (2010).
24. Tan, X. *et al.* Mechanism of auxin perception by the TIR1 ubiquitin ligase. *Nature* **446,** 640–645 (2007).
25. Kikuchi, Y., Shimatake, H. & Kikuchi, A. A yeast gene required for the G1-to-S transition encodes a protein containing an A-kinase target site and GTPase domain. *EMBO J.* **7,** 1175–1182 (1988).
26. Chauvin, C., Salhi, S. & Jean-Jean, O. Human eukaryotic release factor 3a depletion causes cell cycle arrest at G1 phase through inhibition of the mTOR pathway. *Mol. Cell. Biol.* **27,** 5619–5629 (2007).
27. Deshaies, R. J. Protein degradation: prime time for PROTACs. *Nat. Chem. Biol.* **11,** 634–635 (2015).
28. Winter, G. E. *et al.* Drug development. Phthalimide conjugation as a strategy for *in vivo* target protein degradation. *Science* **348,** 1376–1381 (2015).
29. Lu, J. *et al.* Hijacking the E3 ubiquitin ligase cereblon to efficiently target BRD4. *Chem. Biol.* **22,** 755–763 (2015).
30. Petzold, G., Fischer, E. S. & Thomä, N. H. Structural basis of lenalidomide-induced CK1α degradation by the CRL4(CRBN) ubiquitin ligase. *Nature* **532,** 127–130 (2016).

Supplementary Information is available in the online version of the paper.

Acknowledgements Thanks to G. Reyes, C. Havens, P. Jackson and H. Hadjivassiliou for discussions relating to this manuscript, and P. Jackson, J. Hansen, M. Correa, B. Fahr, M. Abbasian, E. Ambing, E. Rychak, D. Mendy and K. Hughes for technical assistance. We thank K. Motamedchaboki (Proteomics Core, Sanford Burnham Prebys Medical Discovery Institute) for mass spectrometry-based proteomic analysis. Thanks to J. Ballesteros and P. Hernandez at Vivia for patient sample testing. Parts of this work were conducted at the Advanced Light Source. The Berkeley Center for Structural Biology is supported in part by the National Institutes of Health, National Institute of General Medical Sciences, and the Howard Hughes Medical Institute. The Advanced Light Source is supported by the Director, Office of Science, Office of Basic Energy Sciences, of the US Department of Energy under contract No. DE-AC02-05CH11231. This work was also supported by Grant-in-Aid for Scientific Research on Innovative Areas "Chemical Biology of Natural Products" from the Ministry of Education, Culture, Sports, Science and Technology (MEXT) (23102002 to H.H.), by JST, PRESTO (T.I.) and by Grant-in-Aid for Young Scientists (B) from MEXT (26750374 to T.I.).

Author Contributions M.E.M., P.P.C., B.P, W.F., J.H., T.I., G.C., and M.R. performed biochemical and crystallographic structural studies. G.L., C.-C.L., K.M., N.-Y.W., D.N., T.T., S.G., and S.X. performed molecular and cellular biology experiments. G.C.L, L.N., M.E.M, and P.P.C. performed electron microscopy studies. A.L.R. performed chemical synthesis. M.E.M., G.L., A.L.-G., J.C., T.I., H.H., T.O.D., B.C., and P.P.C. planned the work, and all authors contributed to the manuscript.

Author Information Coordinates for the structure of cereblon–DDB1–CC-885–GSPT1 have been deposited in the Protein Data Bank with the accession code 5HXB. Reprints and permissions information is available at www.nature.com/reprints. The authors declare competing financial interests: details are available in the online version of the paper. Readers are welcome to comment on the online version of the paper. Correspondence and requests for materials should be addressed to P.P.C. (pchamberlain@celgene.com) or G.L. (glu@celgene.com).

METHODS

Data reporting. No statistical methods were used to predetermine sample size. The experiments were not randomized and the investigators were not blinded to allocation during experiments and outcome assessment.

Protein expression and purification. ZZ-domain-6×His-thrombin-tagged human cereblon (amino acids 40–442) and full-length human DDB1 were co-expressed in SF9 insect cells in ESF921 medium (Expression Systems), in the presence of 50 μM zinc acetate. Cells were resuspended in buffer containing 50 mM Tris-HCl (pH 7.5), 500 mM NaCl, 10 mM imidazole, 10% glycerol, 2 mM TCEP, 1× Protease Inhibitor Cocktail (San Diego Bioscience), and 40,000 U Benzonase (Novagen), and sonicated for 30 s. Lysate was clarified by high speed spin at 108,800*g* for 30 min, and clarified lysate was incubated with Ni-NTA affinity resin (Qiagen) for 1 h. Complex was eluted with buffer containing 500 mM imidazole, and the ZZ-domain-6×His tag removed by thrombin cleavage (Enzyme Research) overnight, combined with dialysis in 10 mM imidazole buffer. Cleaved eluate was incubated with Ni-NTA affinity resin (Qiagen), and the flow-through diluted to 200 mM NaCl for further purification over an ANX HiTrap ion exchange column (GE Healthcare). The ANX column was washed with ten column volumes of 50 mM Tris-HCl (pH 7.5), 200 mM NaCl, 3 mM TCEP, followed by ten column volumes of 50 mM Bis-Tris (pH 6.0), 200 mM NaCl, 3 mM TCEP, and the cereblon–DDB1 peak eluted at 210 mM NaCl. This peak was collected and further purified by size-exclusion chromatography using a Sephacryl S-400 16/60 column (GE Healthcare) in buffer containing 10 mM HEPES (pH 7.0), 240 mM NaCl, and 3 mM TCEP. The cereblon–DDB1 complex was concentrated to 30 mg ml^{-1} for crystallization trials.

GSPT1 domains 2 and 3 (amino acids 437–633) were expressed as an MBP-fusion in *Escherichia coli* BL21 (DE3) Star cells (Life Technologies) using 2XYT media (Teknova). Cells were induced at optical density OD_{600} 0.6 for 18 h at 16 °C. Cells were pelleted, resuspended in buffer containing 200 mM NaCl, 50 mM Tris (pH 7.5), 1 mM TCEP, 10% glycerol, 0.01 mg ml^{-1} lysozyme (Sigma), 10,000 U benzonase (Novagen), and 1× protease inhibitor cocktail (San Diego Bioscience). Resuspended cells were frozen, thawed for purification, and sonicated for 30 s before high speed spin at 108,800*g* for 30 min. Clarified lysate was incubated with amylose resin (NEB) at 4 °C for 1 h before beads were washed with 500 ml wash buffer containing 200 mM NaCl, 50 mM Tris (pH 7.5), 1 mM TCEP, 10% glycerol. Protein was eluted with buffer containing 10 mM maltose, and the MBP tag was removed by overnight cleavage with thrombin (Enzyme Research). Cleaved GSPT1 was diluted into buffer containing 90 mM NaCl and further separated over a Heparin HiTrap column (GE healthcare). The GSPT1 peak eluting at 100 mM NaCl was collected, concentrated, and further separated by size exclusion chromatography using a Superdex 75 16/600 column (GE Healthcare) in buffer containing 10 mM HEPES pH 7, 240 mM NaCl, and 3 mM TECP. The peak containing GSPT1 domains 2 and 3 eluted at 75 ml and was concentrated to 16 mg ml^{-1} for crystallization trials.

MBP–Ikaros 140–168 and mutants were expressed in *E.coli* BL21 (DE3) Star cells (Life Technologies) using 2XYT media (Teknova). Cells were induced at OD_{600} 0.6 for 18 h at 16 °C. Cells were pelleted, resuspended in buffer containing 200 mM NaCl, 50 mM Tris (pH 7.5), 3 mM TCEP, 10% glycerol, 150 μM zinc acetate, 0.01 mg ml^{-1} lysozyme (Sigma), 40,000 U benzonase (Novagen), and 1× protease inhibitor cocktail (San Diego Bioscience). Resuspended cells were frozen, thawed for purification, and sonicated for 30 s before high-speed spin at 108,800*g* for 30 min. Clarified lysate was incubated with amylose resin (NEB) at 4 °C for 1 h before beads were washed. Protein was eluted with buffer containing 200 mM NaCl, 50 mM Tris (pH 7.5), 3 mM TCEP, 10% glycerol, 150 μM zinc acetate, and 10 mM maltose. Eluate was concentrated and further purified by size exclusion chromatography over a Superdex 200 16/600 column (GE Healthcare) in buffer containing 200 mM NaCl, 50 mM Tris (pH 7.5), 3 mM TCEP, 10% glycerol, and 150 μM zinc acetate.

GST–GSPT1 domain 3 (amino acids 526–633) and mutants were expressed in *E.coli* BL21 (DE3) Star cells (Life Technologies) using 2XYT media (Teknova). Cells were induced at OD_{600} 0.6 for 18 h at 16 °C. Cells were pelleted, resuspended in buffer containing 200 mM NaCl, 50 mM Tris (pH 7.5), 3 mM TCEP, 10% glycerol, 0.01 mg ml^{-1} lysozyme (Sigma), 20,000 U benzonase (Novagen), and 1× protease inhibitor cocktail (San Diego Bioscience). Resuspended cells were frozen, thawed for purification, and sonicated for 30 s before high-speed spin at 108,800*g* for 30 min. Clarified lysate was incubated with Glutathione Sepharose 4 Fast Flow (GE Healthcare) at 4 °C for 2 h before beads were washed. Protein was eluted with buffer containing 200 mM NaCl, 50 mM Tris (pH 7.5), 3 mM TCEP, 10% glycerol, and 20 mM reduced glutathione. Eluate was concentrated and further purified by size-exclusion chromatography over a Superdex 200 16/600 column (GE Healthcare) in buffer containing 200 mM NaCl, 50 mM Tris (pH 7.5), 3 mM TCEP, and 10% glycerol.

6×His–eRF1 (human, full length) was expressed in *E. coli* BL21 (DE3) Star cells (Life Technologies) using 2XYT media (Teknova). Cells were induced at OD_{600} 0.6 for 18 h at 16 °C. Cells were pelleted, resuspended in buffer containing 150 mM NaCl, 50 mM Tris (pH 7.5), 3 mM TCEP, 10% glycerol, 0.01 mg ml^{-1} lysozyme (Sigma), 20,000 U benzonase (Novagen), and 1× protease inhibitor cocktail (San Diego Bioscience). Resuspended cells were frozen, thawed for purification, and sonicated for 30 s before high speed spin at 108,800*g* for 30 min. Clarified lysate was incubated with Ni-NTA affinity resin (Qiagen) at 4 °C for 1 h before beads were washed. Protein was eluted with buffer containing 150 mM NaCl, 50 mM Tris (pH 7.5), 3 mM TCEP, 10% glycerol, and 500 mM imidazole. Eluate was concentrated and further purified by size-exclusion chromatography over a Superdex 200 16/600 column (GE Healthcare) in buffer containing 150 mM NaCl, 50 mM Tris (pH 7.5), 3 mM TCEP, and 10% glycerol.

6×His–DDB1 (human, full length) was expressed in SF9 insect cells in ESF921 medium (Expression Systems). Cells were resuspended in buffer containing 50 mM Tris-HCl (pH 7.5), 500 mM NaCl, 10 mM imidazole, 10% glycerol, 2 mM TCEP, 1× Protease Inhibitor Cocktail (San Diego Bioscience), and 40,000 U Benzonase (Novagen), and sonicated for 30 s. Lysate was clarified by high-speed spin at 108,800*g* for 30 min, and clarified lysate was incubated with Ni-NTA affinity resin (Qiagen) for 1 h. Complex was eluted with buffer containing 500 mM imidazole. Eluate was collected and further purified by size-exclusion chromatography over a Superdex 200 16/600 column (GE Healthcare) in buffer containing 150 mM NaCl, 50 mM Tris (pH 7.5), 3 mM TCEP, and 10% glycerol.

The V protein of simian virus 5 (SV5-V) (full length) was expressed in *E. coli* BL21 (DE3) Star cells (Life Technologies) using 2XYT media (Teknova) as a GST-fusion protein. Cells were induced at OD_{600} 0.6 for 18 h at 16 °C. Cells were pelleted, resuspended in buffer containing 150 mM NaCl, 50 mM Tris (pH 7.5), 3 mM TCEP, 10% glycerol, 0.01 mg ml^{-1} lysozyme (Sigma), 20,000 U benzonase (Novagen), and 1× protease inhibitor cocktail (San Diego Bioscience). Resuspended cells were frozen, thawed for purification, and sonicated for 30 s before high speed spin at 108,800*g* for 30 min. Clarified lysate was incubated with Glutathione Sepharose 4 Fast Flow (GE Healthcare) at 4 °C for 2 h before beads were washed and protein eluted with buffer containing 150 mM NaCl, 50 mM Tris (pH 7.5), 3 mM TCEP, 10% glycerol, and 20 mM reduced glutathione. One half of the eluate was incubated with thrombin to remove the GST tag, while the other half retained the tag. Tagged and un-tagged proteins were further purified by size-exclusion chromatography over a Superdex 200 16/600 column (GE Healthcare) in buffer containing 150 mM NaCl, 50 mM Tris (pH 7.5), 3 mM TCEP, and 10% glycerol.

SV5-V–DDB1 complex for the *in vitro* ubiquitination assay was generated by incubating stoichiometric amounts of purified, un-tagged SV5-V and purified 6×His–DDB1 overnight at 4 °C before purification of the complex by separation over a Superdex 200 16/600 column (GE Healthcare) in buffer containing 150 mM NaCl, 50 mM Tris (pH 7.5), 3 mM TCEP, and 10% glycerol.

Negative stain electron microscopy analysis of GSPT1 binding to cereblon–DDB1–CC-885. To prepare grids for negative stain analysis of isolated cereblon–DDB1 or cereblon–DDB1 bound to CC-885 and GST–GSPT1 domains 2 and 3 (amino acids 437–633), pre-incubated protein complex samples were rapidly diluted from 30 μM to 0.3 μM in a buffer containing 50 mM Tris (pH 7.5), 150 mM NaCl, and 1 mM TCEP. A 4 μl aliquot was applied to freshly plasma-cleaned 400 mesh Cu-Rh maxtaform grids (Electron Microscopy Sciences) that had been coated with a thin layer of carbon. After incubating for 1 min, excess protein was wicked off with Whatman filter paper and the grid was immediately inverted and placed on a 50 μl droplet of 2% (w/v) uranyl formate solution. After 30 s, excess stain was wicked off from the grid by touching the edge with filter paper. This staining step was repeated three times for thorough embedding of the sample, and the grids were air dried on the edge of a fume hood for constant air flow after the last blotting step. Samples were imaged on a Tecnai Spirit operating at 120 keV. Data were collected using the Leginon automated image acquisition software (PMID 15890530), and analysed using the Appion processing package (PMID 9263523).

Crystallization and structure determination. Crystallization of the complex was achieved by sitting-drop vapour diffusion. Cereblon–DDB1 and GSPT1 were mixed together to equimolar stoichiometry at a final concentration of 150 μM. The solution of cereblon–DDB1–GSPT1 in the presence of 500 μM CC-885 was mixed 1:1 with, and subsequently equilibrated against, a mother liquor solution of 200 mM sodium citrate, Tris (pH 8.4–8.6), 17–20% PEG 3350 and incubated at 9 °C. Crystals were cryoprotected in the reservoir solution supplemented with 20% ethylene glycol and cooled under liquid nitrogen. Data was collected from a single crystal at the Advanced Light Source, beamline 5.0.2. The structure of human cereblon–DDB1–GSPT1–CC-885 was solved by molecular replacement using Phaser[31], with human cereblon–DDB1 (PDB code 4TZ4) and GSPT1 (PDB code 3E1Y) as search models. Subsequent manual model building using Coot and refinement were performed using Refmac5 with non-crystallographic symmetry and external structure restraints[32,33]. Crystallographic statistics are summarized

in Extended Data Table 1, sample electron density is shown in Extended Data Fig. 7d. Ikaros was modelled on the basis of sequence homology to coordinates with the Protein Data Bank accession number 2I13.

Surface plasmon resonance binding assay. Binding kinetics were measured using a Biacore T200. Using the GST-capture kit (GE Healthcare, BR-1002-23), ~2000 relative units (RU) of anti-GST antibody was immobilized on a CM5 chip (GE Healthcare). GST–GSPT1 domains 2 and 3 (0.07 μg ml^{-1}) or GST (0.15 μg ml^{-1}, reference channel) was then flowed over the chip at 10 μl min^{-1} for 2 min, resulting in a capture level of approximately 10 RU. A threefold dilution series of cereblon–DDB1 (3 μM to 3 nM) was then flowed over both channels at a rate of 30 μl min^{-1} for 300 s contact time, followed by 900 s dissociation time. After each cycle of binding and dissociation, the surface was regenerated with 10 mM glycine (pH 2.1) for 120 s at 30 μl min^{-1}, followed by 3 M $MgCl_2$ for 60 s at 30 μl min^{-1}. All reagents (GST, GST–GSPT1 domain 2 and 3, cereblon–DDB1, and running buffer) were in 10 mM HEPES (pH 7.4), 150 mM NaCl, 0.05% v/v Surfactant P20 containing 0.02% DMSO and saturating levels of the relevant compound, glutarimide or CC-885 (CC-885 at 10 μM, glutarimide at 100 μM). The apparent on- and off-rate constants were globally fit with a 1:1 kinetic binding model to the sensograms (black lines) using the Biacore T200 kinetic analysis software package.

Pull-down binding assays of cereblon and substrates using purified recombinant components. Pull-down of cereblon–DDB1 with either GSPT1 or Ikaros was performed using the same protocol. Tagged substrate, either GST–GSPT1–domain 3 (amino acids 526–633) or MBP–Ikaros (amino acids 140–168), was expressed in bacteria and purified using affinity and size-exclusion chromatography. Substrate was then bound to magnetic glutathione (Pierce) or amylose (NEB) beads for 1 h. Beads were washed three times in pull-down buffer (50 mM Tris pH 7.5, 150 mM NaCl, 10% glycerol, 0.01% NP-40, and 1 mM TCEP, with the addition 150 μM zinc acetate for Ikaros) to remove excess unbound substrate, before the addition of DMSO or 100 μM compound and 50 μM cereblon–DDB1, purified from insect cells using affinity, ion exchange, and size-exclusion chromatography. After 1 h incubation with occasional gentle mixing at room temperature, unbound cereblon–DDB1 was removed and beads were washed three times in pull-down buffer, for a total of 30 s. Substrate and bound cereblon–DDB1 was eluted using either 20 mM reduced glutathione or 10 mM maltose, separated by SDS–PAGE, and Coomassie stained.

Tagged GST–GSPT1 domains 2 and 3 (amino acids 437–633) was expressed in bacteria and purified using affinity and size-exclusion chromatography. GST or GST–GSPT1 domains 2 and 3 was then bound to magnetic glutathione (Pierce) beads for 1 h. Beads were washed 3 times in pull-down buffer (50 mM Tris pH 7.5, 150 mM NaCl, 10% glycerol, 0.01% NP-40, and 1 mM TCEP) to remove excess unbound substrate, before the addition of DMSO or 100 μM compound and 50 μM cereblon–DDB1, purified from insect cells using affinity, ion exchange, and size-exclusion chromatography. After 1 h incubation with occasional gentle mixing at room temperature, unbound cereblon–DDB1 was removed and beads were washed three times in pull-down buffer, for a total of 30 s. Substrate and bound cereblon–DDB1 was eluted using either 20 mM reduced glutathione, separated by SDS–PAGE, and Coomassie stained.

Pull-down of eRF1 or cereblon–DDB1 with GSPT1 domains 2 and 3 and CC-885. Tagged GST–GSPT1 domains 2 and 3 (amino acids 437–633) was expressed in bacteria and purified using affinity and size exclusion chromatography. GST or GST–GSPT1 domains 2 and 3 was then bound to magnetic glutathione (Pierce) beads for 1 h. Beads were washed three times in pull-down buffer (50 mM Tris (pH 7.5), 150 mM NaCl, 10% glycerol, 0.01% NP-40, and 1 mM TCEP) to remove excess unbound substrate, before the addition of DMSO or 100 μM compound and 50 μM purified cereblon–DDB1 or 30 μM purified eRF1, ±CC-885. After 1 h incubation with occasional gentle mixing at room temperature, unbound cereblon–DDB1 or eRF1 was removed and beads were washed three times in pull-down buffer, for a total of 30 s. Substrate and bound cereblon–DDB1 or eRF1 was eluted using either 20 mM reduced glutathione, separated by SDS–PAGE, and Coomassie stained.

Pull-down binding assays of SV5-V, DDB1, and CUL4–RBX1. To confirm that purified SV5-V binds to purified DDB1, and that this complex then binds to CUL4–RBX1, we performed two consecutive GST pull-down assays. GST–SV5-5 or GST alone was purified from bacteria using affinity and size exclusion chromatography. Purified GST–SV5-V or GST was then bound to magnetic glutathione beads (Pierce) for 1 h. Beads were washed three times in pull-down buffer (50 mM Tris (pH 7.5), 150 mM NaCl, 10% glycerol, 0.01% NP-40, and 1 mM TCEP) to remove excess GST–protein, before the addition of purified DDB1. After 1 h of incubation with occasional mixing at room temperature, unbound DDB1 was removed and beads were washed 3 times in pull-down buffer. Substrate and bound DDB1 were then eluted using either 20 mM reduced glutathione, separated by SDS–PAGE, and Coomassie stained. For subsequent binding of CUL4–RBX1, the same pull-down described above was used to generate GST–SV5-V–DDB1 on beads. However, after the beads were washed to remove excess DDB1, CUL4–RBX1 was added and incubated for 1 h at room temperature before beads were washed three times in pull-down buffer and bound protein eluted with 20 mM reduced glutathione, separated by SDS–PAGE, and Coomassie stained.

***In vivo* degradation of cereblon substrates.** 293FT (Invitrogen) *CRBN*$^{-/-}$ cells transiently transfected with plasmids expressing V5-tagged IKZF1, Flag-tagged Ikaros (IKZF3), Myc-tagged GSPT1, GFP and human or mouse cereblon variants. 36 h after transfection, cells were treated with DMSO, 10 μM lenalidomide, or 1 μM CC-885 for an additional 12 h. Cells were then washed with ice-cold 1× PBS twice, lysed in buffer A (50 mM Tris-HCl, 150 mM NaCl, 1% Triton-X 100, complete protease inhibitor tablet (Roche), phosphatase inhibitor tablet (Roche)). Whole-cell extracts were collected and subjected to immunoblot analysis.

Mammalian lysate co-immunoprecipitation. 293FT (Invitrogen) *CRBN*$^{-/-}$ cells were transiently transfected with plasmids expressing Flag-tagged cereblon variants and HA-tagged GSPT1(or HA-tagged IKZF1). After 2 days, cells were lysed in Buffer B (50 mM Tris (pH 7.4), 150 mM NaCl, 0.5% NP-40, 10% glycerol, 1× Complete Ultra protease inhibitor (Roche), and 1× PhosphoSTOP (Roche)). Whole-cell extracts were collected after centrifugation at 16,000*g* for 10 min. Whole-cell extracts containing cereblon and GSPT1 (or IKZF1) were then incubated with anti-HA affinity resin (Roche) in the presence of DMSO or 10 μM CC-885 (or 10 μM lenalidomide). For testing the interaction between cereblon variants and DDB1, whole-cell extracts expressing Flag–CRBN were incubated with anti-Flag affinity resin (Sigma) . After overnight incubation at 4 °C, anti-Flag and anti-HA resins were washed with Buffer B six times. Anti-Flag and anti-HA immunoprecipitates were then subjected to immunoblot analysis.

Cell culture and materials. Human embryonic kidney cell lines 293FT (Invitrogen), 293T (ATCC) and Lenti-X 293 (Clontech) were maintained in Dulbecco's Modified Eagle's medium (DMEM; Invitrogen) supplemented with 10% fetal bovine serum (FBS; Invitrogen), 1× sodium pyruvate (Invitrogen), 1× non-essential amino acids (Invitrogen), 100 U ml^{-1} penicillin (Invitrogen), and 100 μg ml^{-1} streptomycin (Invitrogen). Acute myeloid leukaemia cell lines KG-1, Kasumi-1, U937, MOLM-13, HL-60, and MV-4-11 were purchased from American Tissue Culture Collection (ATCC). NB-4, HNT-34, OCI-AML2, and OCI-AML3 cell lines were purchased from Deutsche Sammlung von Mikroorganismen und Zellkulturen GmbH. KG-1, Kasumi-1, U937, MOLM-13, NB-4, and HNT-34 cell lines were maintained in Roswell Park Memorial Institute (RPMI) 1640 tissue culture medium (Invitrogen) supplemented with 10% FBS, 1× sodium pyruvate, 1× non-essential amino acids, 100 U ml^{-1} penicillin, and 100 μg ml^{-1} streptomycin. HL-60 and MV-4-11 cell lines were maintained in Iscove's Modified Dulbecco's medium (IMDM; (Invitrogen) supplemented with 10% FBS, 1× sodium pyruvate, 1× non-essential amino acids, 100 U ml^{-1} penicillin, and 100 μg ml^{-1} streptomycin. OCI-AML2 and OCI-AML3 cell lines were maintained in minimal essential medium (MEM; Invitrogen) supplemented with 10% FBS, 1× sodium pyruvate, 1× non-essential amino acid, 100 U ml^{-1} penicillin, and 100 μg ml^{-1} streptomycin. All cell lines were cultured at 37 °C with 5% CO_2 in the relevant media mentioned above. All cell lines were confirmed to be mycoplasma-negative using the MycoAlert Mycoplasma Detection Kit (Lonza).

Cell proliferation assay. Human cancer cell lines cultured in the growth medium recommended by the vendor were seeded into black 384-well plates containing DMSO or test compounds. The seeding density for each cell line was optimized to allow the cell growth in the linear range during a 3-day culture period. To test the compound effect on cell proliferation in AML cell lines, 5,000 to 10,000 cells per well in 200 μl complete culture media were seeded into black 96-well plates containing DMSO or test compounds. After 48 or 72 h, cell proliferation was assessed using the CellTiter-Glo (CTG) Luminescent Cell Viability Assay (Promega) according to manufacturer's instructions. To test the effect of GSPT1 depletion on cell proliferation in AML cell lines, cells were infected with lentiviral shRNA vectors for 4 days, and cell proliferation was quantified using CTG every other day thereafter. Relative cell proliferation was normalized against day 4 cell growth values. To determine the effect of GSPT1 depletion on cell proliferation in 293T HEK cells, cells were infected with lentiviral shRNA vectors for 7 days, and then imaged using the EVOS FL Cell Imaging System (Thermo Fisher). The effect of CC-885 on AML patient-derived cells was performed by automated flow cytometry according to the methods described in ref. 34. Briefly, patient-derived bone marrow samples from adult patients over 18 years of age who were diagnosed with AML, were obtained from Hospital La Fe, Hospital General Universitario Gregorio Marañon and Hospital Lucus Augusti hospitals, all in Spain, following IRB approved protocols and signed informed consent. Bone marrow samples were extracted under sterile conditions and were received in the laboratory within 24 h of extraction where they were immediately processed. A small portion of the sample was separated for validation and selection of the monoclonal antibodies (mAb) to optimize the identification of leukaemic cells. The majority of the sample was diluted with culture media and plated into 96-well plates previously prepared with the test compounds. These plates were incubated for 24, 48 and 96 h and then

processed via the ExviTech platform. For this purpose, red cells were lysed and leukocytes were stained using the mAb previously selected and with Anexin-V to exclude apoptotic cells.

Antibodies. Rabbit anti-human CRBN65 mAb (Celgene, San Diego, CA)[3], rabbit anti-DYKDDDDK (Flag) (9A3) mAb (#8146, Cell Signaling), mouse anti-Myc-Tag (9B11) mAb (#2276, Cell Signaling), mouse anti-GFP (B-2) mAb (#sc-9996, Santa Cruz), rabbit anti-human GSPT1 polyclonal antibody (pAb) (ab49878, Abcam), rabbit anti-human GSPT1 pAb (ab126090, Abcam), rabbit anti-GSPT1 pAb (10763-1-AP, Proteintech), rabbit anti-Ikaros (D10E5) mAb (#9034, Cell signaling), mouse anti-HA.11 (16B12) mAb (#901501, Biolegend), rabbit anti-DDB1 pAb (#5428, Cell Signaling), mouse anti-ubiquitin P4D1 mAb (#SC-8017, Santa Cru), mouse anti-SV5-V (Santa Cruz, sc-58052), mouse anti-HIS mAb antibody (34660, Qiagen), mouse anti- actin mAb (#A5316, Sigma) and mouse anti-tubulin mAb (#T5201, Sigma) were used as primary antibodies. Goat anti-mouse 800 antibody (#926-32210, LICOR Biosciences), goat anti-rabbit 680 antibody (#926-68071, LI-COR Biosciences), goat anti-mouse 680 antibody (#926-68070, LI-COR Biosciences) and goat anti-rabbit 800 antibody (#926-32211, LI-COR Biosciences) were used as secondary antibodies.

Cellular immunoprecipitation. Cells were lysed in Buffer B (50 mM Tris (pH 7.4), 150 mM NaCl, 0.5% NP-40, one tablet of Complete ULTRA protease inhibitor cocktail (Roche), and one tablet of PhosSTOP phosphatase inhibitor cocktail (Roche)). Whole-cell lysates were clarified by centrifugation at top speed for 10 min. To identify cereblon-associated proteins, CC-885 (2 μM) or DMSO were added into whole cell extracts of 293T HEK cells stably expressing Flag–HA–CRBN for 2 h. FH–CRBN complexes were then captured with anti-Flag beads (Sigma), eluted by Flag peptide, and separated on SDS–PAGE gel, followed by mass spectrometry or immunoblot analysis. To test the binding of cereblon to its substrates, 293FT HEK cells stably expressing HA-tagged GSPT1, IKZF1, IKZF1(Q146H) were lysed in Buffer B. HA-tagged recombinant proteins were then immunoprecipitated with anti-HA beads (Roche). After three washes with Buffer B, the anti-HA beads were mixed with cell lysates of 293FT HEK cells stably expressing shGSPT1-1 in the presence of DMSO, 10 μM lenalidomide or 10 μM CC-885 for 12 h. To test the binding of HA-tagged GSPT1 variants with cereblon and eRF1, whole-cell lysates of 293T HEK cells stably expressing GSPT1 variants were treated with DMSO or 20 μM CC-885 for 2 h, followed by anti-HA immunoprecipitation for an additional 4 h. Beads were then washed with Buffer B six times, and bound proteins were eluted by boiling in LDS loading buffer and detected by immunoblot analysis.

Plasmids. Plasmids pDONR221 and pDONR223-IKZF3 were purchased from Invitrogen and assembled to generate pDONR223. Coding sequences of IKZF1, SUP35, GSPT1, cereblon and Flag–HA–cereblon were *in vitro* synthesized by Invitrogen and then cloned into pDONR223. Open reading frames encoding IKZF1(Q146H) and chimaeric fusion proteins of SUP35 and GSPT1 were generated via overlapping PCR, and then cloned into pDONR223. GSPT1 mutations and truncation deletions were introduced into pDONR223-GSPT1 via overlapping PCR. Cereblon mutants E377V and W386A in pDORN223 were generated via overlapping PCR.

DNA fragments of gateway-3×HA–mPGK (mouse phosphoglycerate kinase promoter)-GFP-P2A-Pur-WPRE, 3×HA-gateway-mPGK-Pur-WPRE and gateway-3×HA-mPGK- Pur-WPRE were *in vitro* synthesized by Invitrogen, and assembled into plenti6.2/v5-DEST (Invitrogen) to generate plenti-CMV-gateway-3×HA-mPGK-GFP-P2A-Pur, plenti-CMV-3xHA-gateway-mPGK-Pur and plenti-CMV-gateway-3×HA-mPGK-Pur, respectively. The Ubc promoter from plenti-6/Ubc/V5-DEST (Invitrogen) was used to replace the CMV promoter in plenti-CMV-gateway-3×HA-mPGK-GFP-P2A-Pur, plenti-CMV-3×HA-gateway-mPGK-Pur and plenti-CMV-gateway-3×HA-mPGK-Pur to generate plenti-Ubc-gateway-3×HA-mPGK-GFP-P2A-Pur, plenti-Ubc-3×HA-gateway-3×HA-mPGK-Pur, and plenti-Ubc-gateway-3×HA-mPGK-Pur. The EF1α promoter from pEF-DEST51 (Invitrogen) was cloned into plenti-CMV-gateway-3×HA-mPGK-GFP-P2A-Pur, plenti-CMV-3×HA-gateway-mPGK-Pur and plenti-CMV-gateway-3×HA-mPGK-Pur to generate plenti-EF1α-gateway-3×HA-mPGK-GFP-P2A-Pur, plenti-EF1α-3×HA-gateway-3×HA-mPGK-Pur, and plenti-EF1α-gateway-3×HA-mPGK-Pur.

Next, pDONR233-GSPT1 was shuttled into plenti-CMV-gateway-3×HA-mPGK-GFP-P2A-Pur and plenti-EF1α-gateway-3×HA-mPGK-GFP-P2A-Pur via gateway LR (att L and att R) recombination. Similarly, pDONR223-GSPT1 wild-type and variants, pDONR223-SUP35, as well as pDONR223-GSPT1/SUP35 chimaeric fusion variants were shuttled into plenti-EF1α-3×-HA-mPGK-Pur. pDONR223-Flag–HA–CRBN and pDONR223-CRBN wild-type and mutants were cloned into plenti-CMV-gateway-3×HA-mPGK-GFP-P2A-Pur and plenti-EF1α-gateway-3×HA-mPGK-P2A-Pur. pDONR223-IKZF1, pDONR223-IKZF1-Q146H and pDONR223-GSPT1 was cloned into plenti-Ubc-gateway-3×HA-mPGK-Pur or plenti-Ubc-3×HA-gateway-mPGK-Pur. A stuffer sequence was synthesized *in vitro* by Invitrogen, and cloned into Mission TRC2 pLKO.5-pur empty vector control plasmid (Sigma) to generate pLKO.5pur-Stuffer. Coding sequence of 8×His–Ub was *in vitro* synthesized by Invitrogen and cloned into pcDNA3 to generated pcDNA3-8×His–Ub.

In-gel digestion and sample preparation for LC-MS/MS Analysis. Gel bands were excised and de-stained. Proteins were reduced and alkylated by addition of 50 mM DTT and 50 mM iodoacetamide before digestion by Trypsin at a final concentration of 25 ng μl^{-1} in 50 mM ammonium bicarbonate for 1 h on ice and additionally 16 h more at 37 °C using a shaking incubator to assure complete digestion. Digested tryptic peptides were extracted from gels by addition of 200 μl of water and sonication for 10 min, washed in 5% formic acid in water and extracted in 50% acetonitrile in 5% formic acid in water, once in 70% acetonitrile and last in 100% acetonitrile. All extracted peptides were pooled together and were vacuum-dried and re-dissolved in 20 μl of 0.1% TFA. Tryptic peptides were then concentrated and desalted using a Millipore C18 Zip Tip (Millipore). The eluted peptides were then vacuum-dried and re-dissolved in 100 μl of LC-MS/MS loading buffer (2% acetonitrile in 0.1% formic acid in water).

One-dimensional LC-MS/MS analysis. Tryptic digested samples were subjected to an on-line analysis of peptides by high-resolution, high-accuracy LC-MS/MS, consisting of a Bruker-Michrom paradigm HPLC, a Zorbax C18 peptide trap column (Agilent technologies), a 15-cm Michrom Magic C18 column, a low-flow ADVANCED Michrom MS source, and a LTQ-Orbitrap XL (Thermo Fisher Scientific). The LC-MS/MS raw data were submitted to Sorcerer Enterprise v.3.5 release (Sage-N Research Inc.) with the SEQUEST algorithm to search the target-decoy ipi.Human.v3.73 database. The search results were viewed, sorted, filtered, and statically analysed by using comprehensive proteomics data analysis software, Peptide/Protein prophet v.4.02 (ISB). The differential spectral count analysis was done by QTools (Sanford Burnham).

Lentiviral shRNA. Pairs of synthetic complementary oligonucleotides targeting GSPT1 or a non-mammalian control (shCNTL) were annealed and cloned into pLKO.5pur-Stuffer. Targeting sequences are listed below: shCNTL, 5′-CAACAAGATGAAGAGCACCAA-3′; shGSPT1-1, 5′-GATTACCGTTTATTCCATA-3′; shGSPT1-2, 5′-CCGATGATGTAGAGACTGATA-3′; shGSPT1-3, 5′-CCTGCACAATACTGTGAGGAA-3′; shGSPT1-4, 5′-GCCGAACTTCAATAGATCAGT-3′.

Protein half-life analysis. 293FT HEK parental and *CRBN*$^{-/-}$ cells were pretreated with DMSO or CC-885 (10 μM) for 30 min, followed by the addition of 100 μg ml^{-1} cycloheximide (EMD) into the culture medium. At various time points, cells were collected and subjected to immunoblot analysis.

***In vivo* ubiquitination assay.** The ubiquitination assays were carried out as described previously[34]. Briefly, 293FT HEK parental or *CRBN*$^{-/-}$ cells cultured in 10-cm plates were transfected with 12 μg of pcDNA3-8×His-Ub. After 48 h, cells were treated with 10 μM CC-885 and 10 μM MG132. Eight hours later, cells were washed twice with ice cold PBS and resuspended in 1 ml PBS. 20 μl of the cell suspension was boiled in LDS loading buffer (Thermo Fisher), and the remaining cells were collected via centrifugation and lysed in Buffer C (6 M guanidine–HCl, 0.1 M Na_2HPO_4/NaH_2PO_4, 20 mM imidazole (pH 8.0)). Next, whole-cell extracts were sonicated for 12 pulses, and mixed with 30 μl of Ni-NTA agarose beads at room temperature for 4 h. Ni-NTA beads were then washed twice with Buffer C, twice with Buffer D (1 volume of Buffer C to 3 volumes of Buffer E), and twice with Buffer E (25 mM Tris HCl, 20 mM imidazole (pH 6.8)). Bound proteins were eluted by boiling in 2× LDS loading buffer and subjected to immunoblot analysis with two mouse anti-GSPT1 monoclonal antibodies 17G9 and 8A2 generated in house (Celgene), a mouse anti-His tag monoclonal antibody (Qiagen #34660, Qiagen) and a rabbit anti-human CRBN monoclonal antibody (CRBN65, Celgene). To detect the ubiqitination of GSPT1, boiled eluates were further diluted with 20 volumes of Buffer B (50 mM Tris (pH 7.4), 150 mM NaCl, 0.5% NP-40, one tablet of Complete ULTRA protease inhibitor cocktail (Roche)), followed by immunoprecipitation with a mouse anti-GSPT1 monoclonal antibody (17G9) immobilized on protein G beads. Beads were washed with Buffer B six times, and bound proteins were eluted by boiling in 1× SDS loading buffer and subjected to immunoblot analysis for GSPT1 with a rabbit anti-GSPT1 antibody (Abcam # 49878) and two rabbit anti-ubiquitin antibodies (Cell Signaling #3933 and Bethyl #A300-317A).

***In vitro* ubiquitination assays.** Purified E1, E2, ubiquitin, CUL4A–RBX1, cereblon–DDB1, and GSPT1 proteins were used to reconstitute the ubiquitination of GSPT1 *in vitro*. Human GSPT1 domains 2 and 3 (amino acids 437–633) was expressed in BL21 star DE3 *E. coli* and purified by maltose affinity resin (NEB), heparin HiTrap column affinity (GE Healthcare), and Superdex 75 16/60 size-exclusion chromatography (GE Healthcare), as described above. Human cereblon–DDB1 (cereblon amino acids 40–442 and full-length DDB1) and 6×his–DDB1 alone were co-expressed in SF9 insect cells in the presence of 50 μM zinc acetate, and purified by nickel affinity resin (Qiagen), HiTrap ANX column ion exchange (GE Healthcare), and Sephacryl 400 16/60 size-exclusion chromatography

(GE healthcare), as described above. SV5-V and DDB1 were purified separately, incubated to form a complex, and the complex purified with size-exclusion chromatography as described above. Human full-length CUL4A and RBX1 were co-expressed in SF9 insect cells and purified by nickel affinity resin and Superdex 200 16/60 size-exclusion chromatography. Purified recombinant human Ube1 E1 (E-305), UbcH5a E2 (E2-616), and ubiquitin (U-100H) were purchased from R&D systems. Components were mixed to final concentrations of 1 μM Ube1, 25 μM UbcH5a, 200 μM Ub, 1 μM CUL4–RBX1, 25 μM GSPT1, and 1 μM cereblon–DDB1, 6×His–DDB1, or SV5-V–DDB1,with or without 100 μM CC-885 in ubiquitination assay buffer (20 mM HEPES (pH 7.5), 150 mM NaCl, 10 mM $MgCl_2$). After preincubation for 10 min at room temperature, ubiquitination reactions were started by addition of ATP to a final concentration of 10 mM. Reactions were incubated at 30 °C for 2 h before separation by SDS–PAGE followed by coomassie staining or immunoblot analysis for GSPT1, ubiquitin, cereblon or SV5-V.

qRT–PCR Analysis. Following incubation with test compounds, cells were collected via centrifugation at 872*g* for 2 min. Cell pellets were then washed once in ice-cold PBS and snap-frozen in liquid nitrogen. Total RNA was extracted using RNeasy Mini Kit (Qiagen) according to manufacturer's instruction, and reverse-transcribed into first-strand cDNA using AffinityScript QPCR cDNA Synthesis Kit (Agilent) with random primer. Real-time PCR was performed in triplicate using ViiA 7 Real-Time PCR System with TaqMan Gene Expression Assay probes (Invitrogen) for GSPT1 (# 4331182) and GAPDH (#4326317E).

Lentiviral production and infection. Lentiviral plasmid was cotransfected with the 2nd Generation packaging system (ABM) into Lenti-X 293 cells using Lipofectamine 2000 (Thermo Fisher). After 12 h of incubation, media was changed to fresh DMEM media supplemented with 20% FBS. At 36 h after transfection, viral supernatant was collected and fresh media was replenished. At 56 h, viral supernatant was collected again, combined with the first viral supernatant, cleared via centrifugation at 872*g* for 5 min, and then filtered through a 0.45 micron cellulose acetate or nylon filter unit. All lentiviral supernatants, except those of lentiviral shRNA vectors, were concentrated using a Lenti-X concentrator according to the manufacturer's instructions. AML cell lines were spin-inoculated with lentivirus at 872*g* for 90 min. After 12 h, viral supernatant was removed and complete culture media was added to the cells. 48 h later, cells were incubated with 1–2 μg ml^{-1} puromycin or 10–20 μg ml^{-1} blasticidin for an additional 3 days to select cells stably integrated with lentiviral vectors.

Data analysis. All cell proliferation assays were independently performed three times with three technical replicates for each sample. All qRT–PCR assays were carried out two times with three technical replicates for each sample. When possible, results were confirmed in multiple cell lines. For quantification of cell proliferation and qRT–PCR, data were analysed using GraphPad Prism and Excel, respectively. $P < 0.05$, unpaired two-sided *t*-test, is considered as significant.

31. McCoy, A. J. *et al.* Phaser crystallographic software. *J. Appl. Crystallogr.* **40,** 658–674 (2007).
32. Emsley, P., Lohkamp, B., Scott, W. G. & Cowtan, K. Features and development of Coot. *Acta Crystallogr. D* **66,** 486–501 (2010).
33. Murshudov, G. N. *et al.* REFMAC5 for the refinement of macromolecular crystal structures. *Acta Crystallogr. D* **67,** 355–367 (2011).
34. Bennett, T. A. *et al.* Pharmacological profiles of acute myeloid leukemia treatments in patient samples by automated flow cytometry: a bridge to individualized medicine. *Clin. Lymphoma Myeloma Leuk.* **14,** 305–318 (2014).

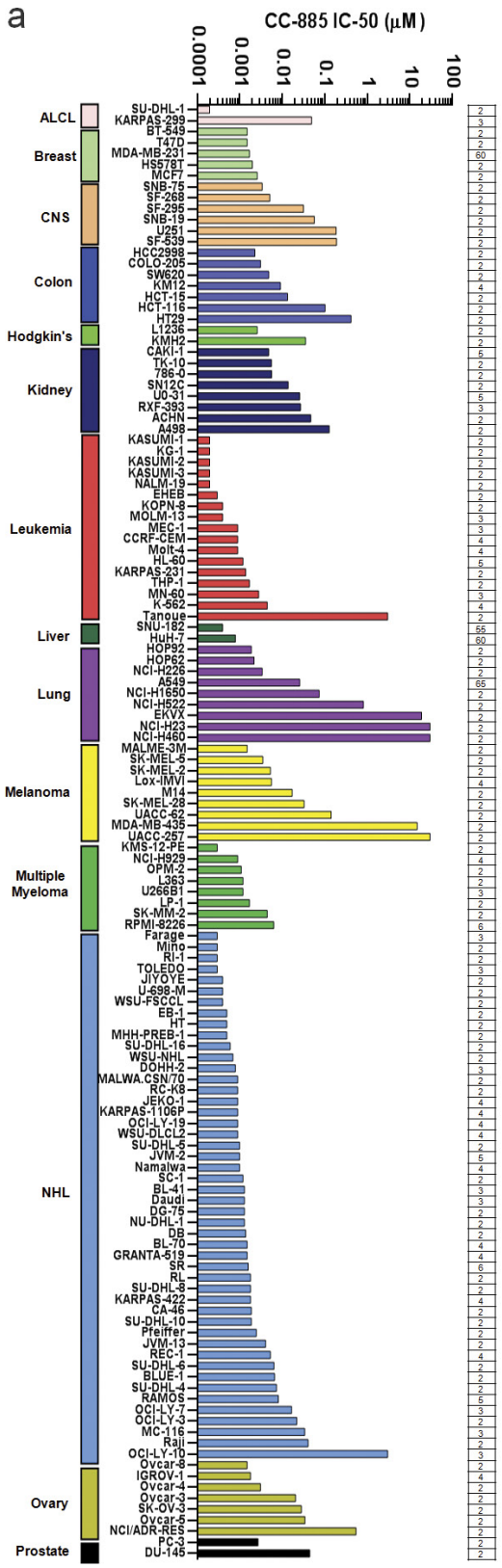

d

	KG-1	KG-1α	KASUMI-1	NB4	MV-4-11	MOLM-13	HL-60	U-937	OCI-AML2	OCI-AML3	THLE-2	PBMC
Lenalidomide (μM)	>10.0	>10.0	>10.0	>10.0	>10.0	>10.0	>10.0	>10.0	>10.0	>10.0	>10.0	>10.0
Pomalidomide (μM)	> 10.0	> 10.0	> 10.0	> 10.0	> 10.0	> 10.0	> 10.0	> 10.0	> 10.0	>10.0	>10.0	>10.0
CC-885 (μM)	0.0007	0.0008	0.0006	0.00006	0.0006	0.0007	0.0005	0.0016	0.0012	0.0016	0.00104	0.0011

Extended Data Figure 1 | See next page for caption.

Extended Data Figure 1 | The anti-tumour effects of CC-885 are CRBN dependent. a, The growth inhibitory IC_{50} value of CC-885 in human cancer cell lines. The cell proliferation of 132 human cancer cell lines treated with varying concentrations of CC-885 for 3 days was assessed by Cell Titre Glo assay. Cancer types as indicated at the bottom are labelled with different colours. The IC_{50} value of growth inhibition was determined using ActivityBase (IDBS). Data are the mean of two or more biological replicates. The *n* number for each cell line is shown on the right of the panel. **b**, The effect of CC-885 on AML samples taken from patients. The top panel shows the effects on leukaemic cells; the bottom panel shows the effects on normal lymphoid cells. The sample from patient B did not contain sufficient normal lymphoid cells for analysis. **c**, The effect of CC-885 on cell proliferation in parental and $CRBN^{-/-}$ 293FT HEK cells. Result is representative of three biological replicates. Data are shown as mean ± s.d., $n = 3$ technical replicates. **d**, The effect of lenalidomide, pomalidomide and CC-885 on cell proliferation in AML cell lines, THLE-2 and human PBMC. Cells were treated with varying concentrations of lenalidomide, pomalidomide or CC-885. At day 3, cell proliferation was assessed using CTG assay. Numbers shown are the growth inhibitory IC_{50} values of lenalidomide, pomalidomide and CC-885, from biological replicates with $n = 5$, 3, and 20, respectively.

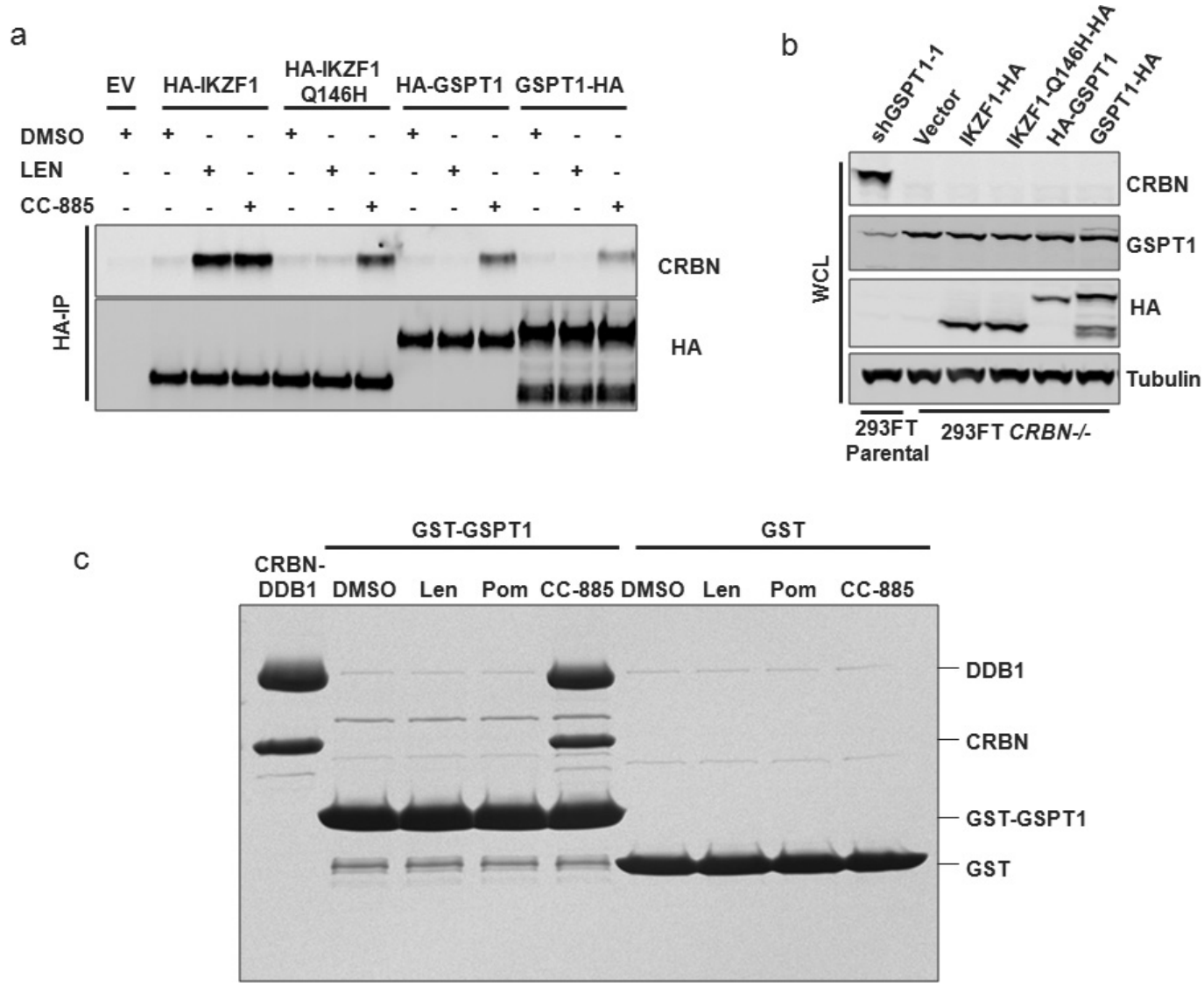

Extended Data Figure 2 | CC-885, but not lenalidomide, promotes the interaction between GSPT1 and CRBN *in vitro*. **a**, **b**, Immunoblot analysis of anti-HA immunoprecipitates (**a**) and whole-cell lysates (WCL) (**b**). HA-tagged GSPT1 or IKZF1 produced in 293FT $CRBN^{-/-}$ HEK cells were used to capture CRBN from 293FT HEK cells expressing GSPT1-specific shRNA, shGPST1-1. DMSO, 10 μM lenalidomide or 10 μM CC-885 were included in the binding assay. The IKZF1 Q146H mutation results in a reduction of cereblon binding mediated by either lenalidomide or CC-885. Some residual binding is observed with CC-885, consistent with Fig. 1d, which shows that CC-885 is more potent than lenalidomide against IKZF1. **c**, Coomassie stain of CRBN–DDB1 pull-down with GSPT1 using purified components. Purified GST or GST–GSPT1 domains 2 and 3 (amino acids 437–633) bound to magnetic glutathione beads was incubated with purified CRBN–DDB1 in the presences of CC-885, lenalidomide (len), pomolidamide (pom), or DMSO (vehicle) for 1 h at room temperature before three rapid washes. CC-885, but not lenalidomide, pomalidomide or DMSO, mediated the binding of GST–GSPT1 to CRBN–DDB1. This experiment was performed three times. For gel source data, see Supplementary Information Fig. 1.

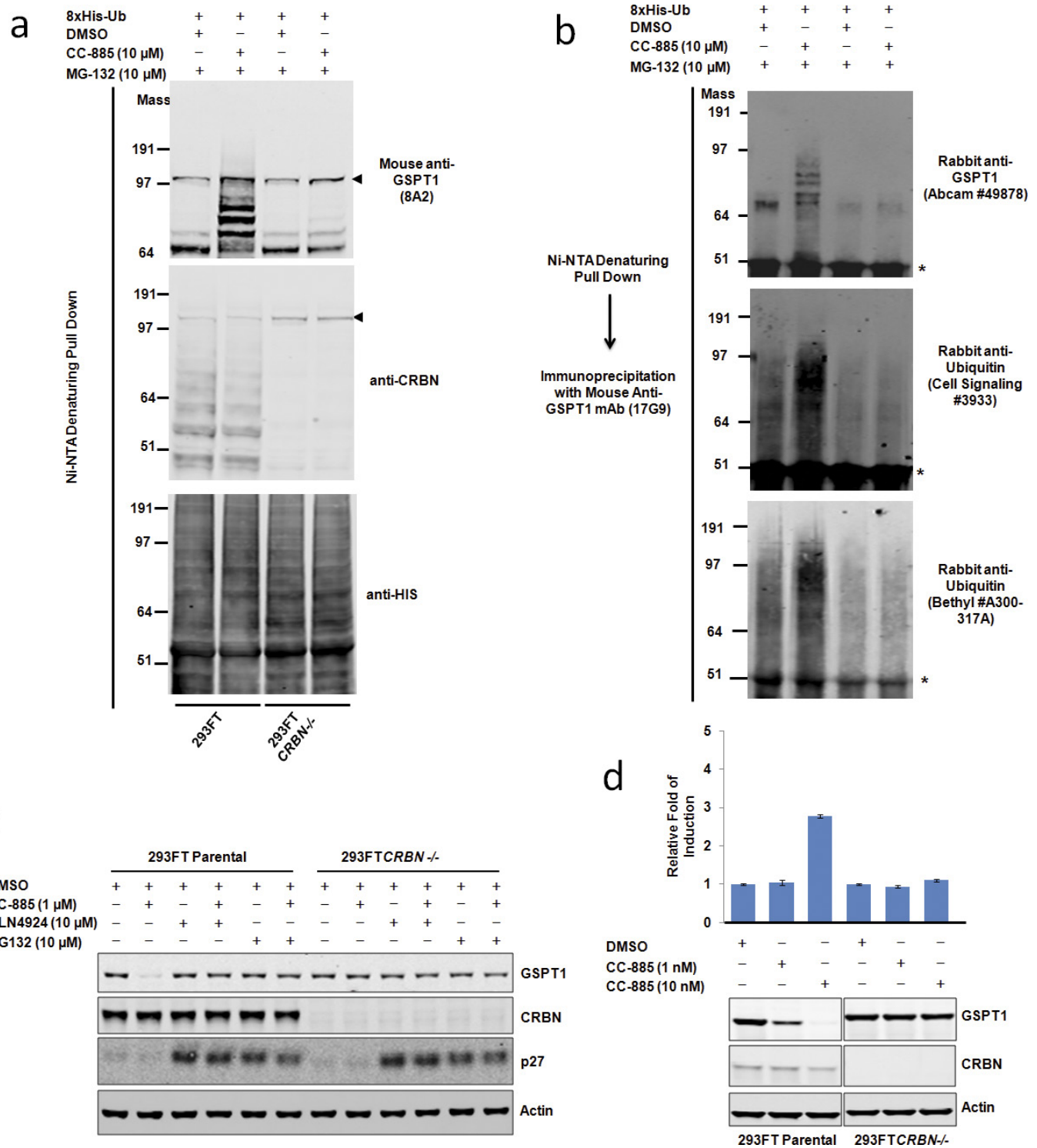

Extended Data Figure 3 | Transcriptional and post-transcriptional regulation of GSPT1 by CC-885. a, Ubiquitinated protein products, as shown in Fig. 1e, were blotted for GSPT1 with mouse anti-GSPT1 monoclonal antibody 8A2, CRBN, and His-tagged Ubiquitin. Arrowheads mark nonspecific bands. **b**, 293FT parental and *CRBN*$^{-/-}$ cells transiently expressing His-tagged ubiquitin was treated with CC-885 and MG132 as indicated for 8 h. Ubiquitinated protein products were pulled down with Ni-NTA agarose under denaturing conditions, followed by elution via boiling in SDS loading buffer. Eluates were diluted with immunoprecipiation buffer and GSPT1 was immunoprecipitated with a mouse anti-GSPT1 monoclonal antibody 17G9. Immunoprecipitates were then subjected to immunoblot analysis for GSPT1 and ubiquitin with two different rabbit anti-ubiquitin antibodies. **c**, Immunoblot analysis of 293FT parental and *CRBN*$^{-/-}$ cells treated with CC-885 for 4 h. Cells were pretreated with DMSO, CC-885, MLN4924 or MG132 as indicated. **d**, 293FT parental or *CRBN*$^{-/-}$ cells treated with DMSO or CC-885 for 24 h were subjected to real-time qPCR (top) and immunoblot analysis (bottom). Result is representative of two biological replicates. Data are mean ± s.d., $n = 3$ technical replicates. For gel source data, see Supplementary Information Fig. 1.

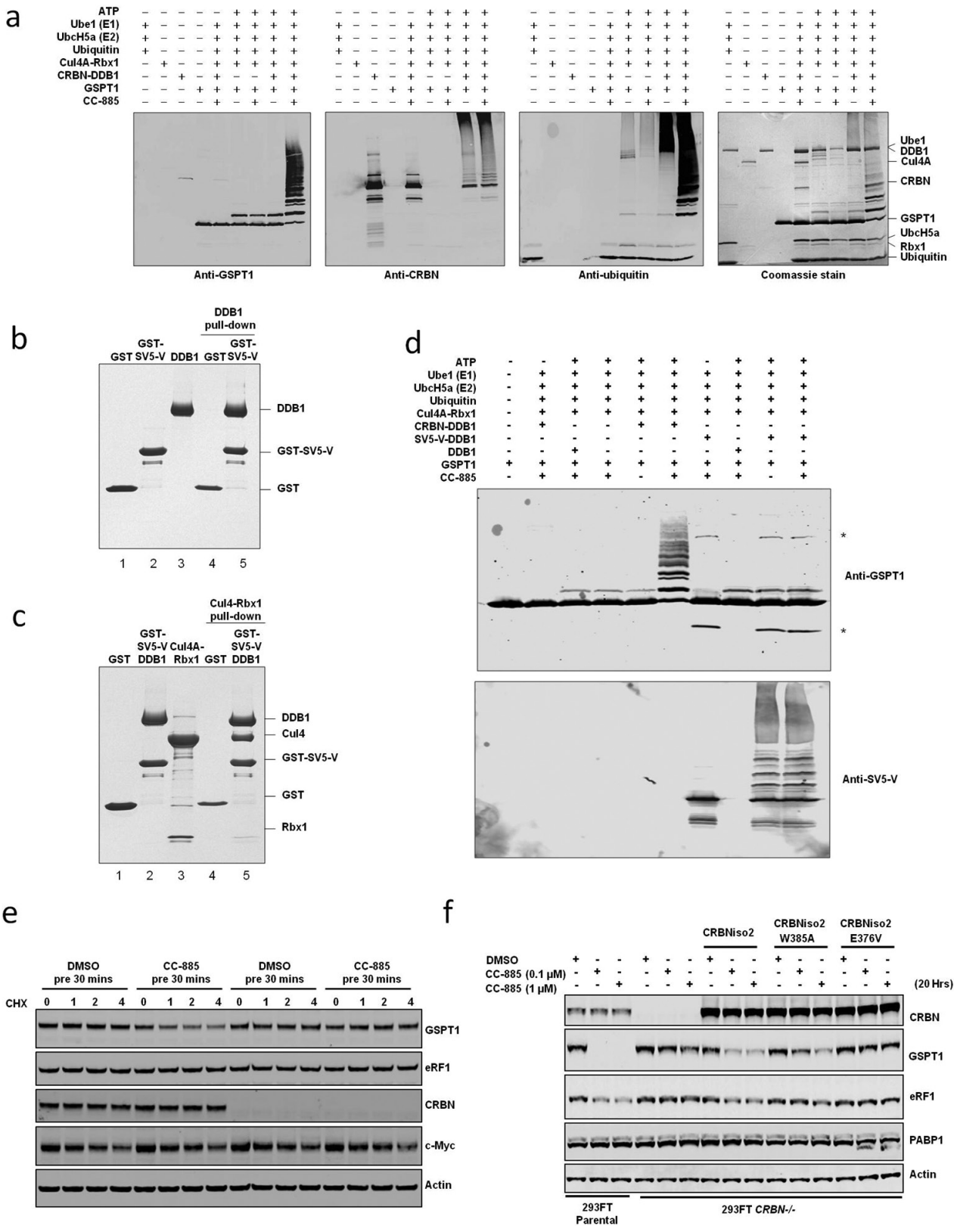

Extended Data Figure 4 | See next page for caption.

Extended Data Figure 4 | The CC-885 induced GSPT1 ubiquitination and degradation relies on CRBN. a, Controls for the *in vitro* ubiquitination assay shown in Fig. 1f. Recombinant protein products as indicated were incubated with or without ATP (10 mM) and CC-885 (100 μM) in the ubiquitination assay buffer at 30 °C for 2 h, and then separated by SDS–PAGE followed by Coomassie staining or immunoblot analysis with anti-GSPT1, anti-cereblon, and anti-ubiquitin antibodies. The anti-GSPT1 blot shown is the same one shown in Fig. 1f. The additional blots and Coomassie staining analysis was performed on samples from the same *in vitro* ubiquitination reactions. Anti-GSPT1 blotting and Coomassie staining was performed three times, anti-cereblon and anti-ubiquitin blotting was performed twice. **b**–**d**, To demonstrate the CRBN-dependence of GSPT1 ubiquitination by CC-885-CRL4, we reconstituted DDB1 with an alternative DCAF, SV5-V, and showed that SV5-V is not capable of recruiting GSPT1 for polyubiquitination. **b**, DDB1 binds to GST–SV5-V, but not GST alone. Coomassie stain with lanes 1, 2, and 3 showing individual proteins, and lanes 4 and 5 showing pull-down of DDB1 incubated with GST or GST–SV5-V bound to glutathione magnetic beads and washed three times. This experiment was performed twice. **c**, GST–SV5-V–DDB1 protein complex generated by pull-down in **b** was used to show binding of CUL4–RBX1 to the GST–SV5-V–DDB1 protein complex but not GST alone. Coomassie stain with lanes 1, 2, and 3 showing individual proteins or protein complexes used in the pull-down, and lanes 4 and 5 showing pull-down of CUL4–RBX1 incubated with GST or GST–SV5-V–DDB1 bound to glutathione magnetic beads and washed three times. This experiment was performed once. **d**, *In vitro* ubiquitination of GSPT1 by CRBN–DDB1 but not SV5-V–DDB1. SV5-V–DDB1 complex was formed by incubation of individually purified proteins and purification over size-exclusion chromatography. Recombinant protein products as indicated were incubated with either CRBN–DDB1, SV5-V–DDB1, DDB1 alone, or the absence of any DDB1 complex, with and without ATP (10 mM) or CC-885 (100 μM) in ubiquitination assay buffer at 30 °C for 2 h, and then separated by SDS–PAGE followed by immunoblot analysis with anti-GSPT1 and anti-SV5-V antibodies. Asterisk indicates background bands present from the SV5-V protein purification. The anti-SV5-V western blot indicates that SV5-V is auto-ubiquitinated, as expected for a functional DCAF that is bound to the DDB1–CUL4–RBX1 complex. **e**, Immunoblot analysis of 293FT parental and *CRBN*$^{-/-}$ cells treated with 100 μg ml^{-1} cyclohexamide (CHX) for the indicated periods. Where indicated, cells were pretreated with DMSO or 10 μM CC-885 for 30 min. This experiment was performed once. **f**, Immunoblot analysis of 293FT parental cells, *CRBN*$^{-/-}$ cells, and *CRBN*$^{-/-}$ cells stably expressing CRBN wild-type or variants as indicated. CRBNiso2 (CRBN isoform 2) showed similar E3 ligase activity towards GSPT1 as compared to CRBN isoform 1 (data not shown). CRBN isoform 2 lacks an alanine residue at position 23 of CRBN isoform 1, and as such the numbering is shifted compared to isoform 1. Note that the CRBN(W385A) mutant showed diminished activity in cells treated with 0.1 μM CC-885, and similar activity in cells treated with 1 μM CC-885, compared to wild-type CRBN. CRBN(E376V) mutant had no activity at both concentrations. Immunoblot analysis of 293FT parental and *CRBN*$^{-/-}$ cells treated with 100 μg ml^{-1} cyclohexamide for the indicated periods. Where indicated, cells were pretreated with DMSO or 10 μM CC-885 for 30 min. For gel source data, see Supplementary Information Fig. 1.

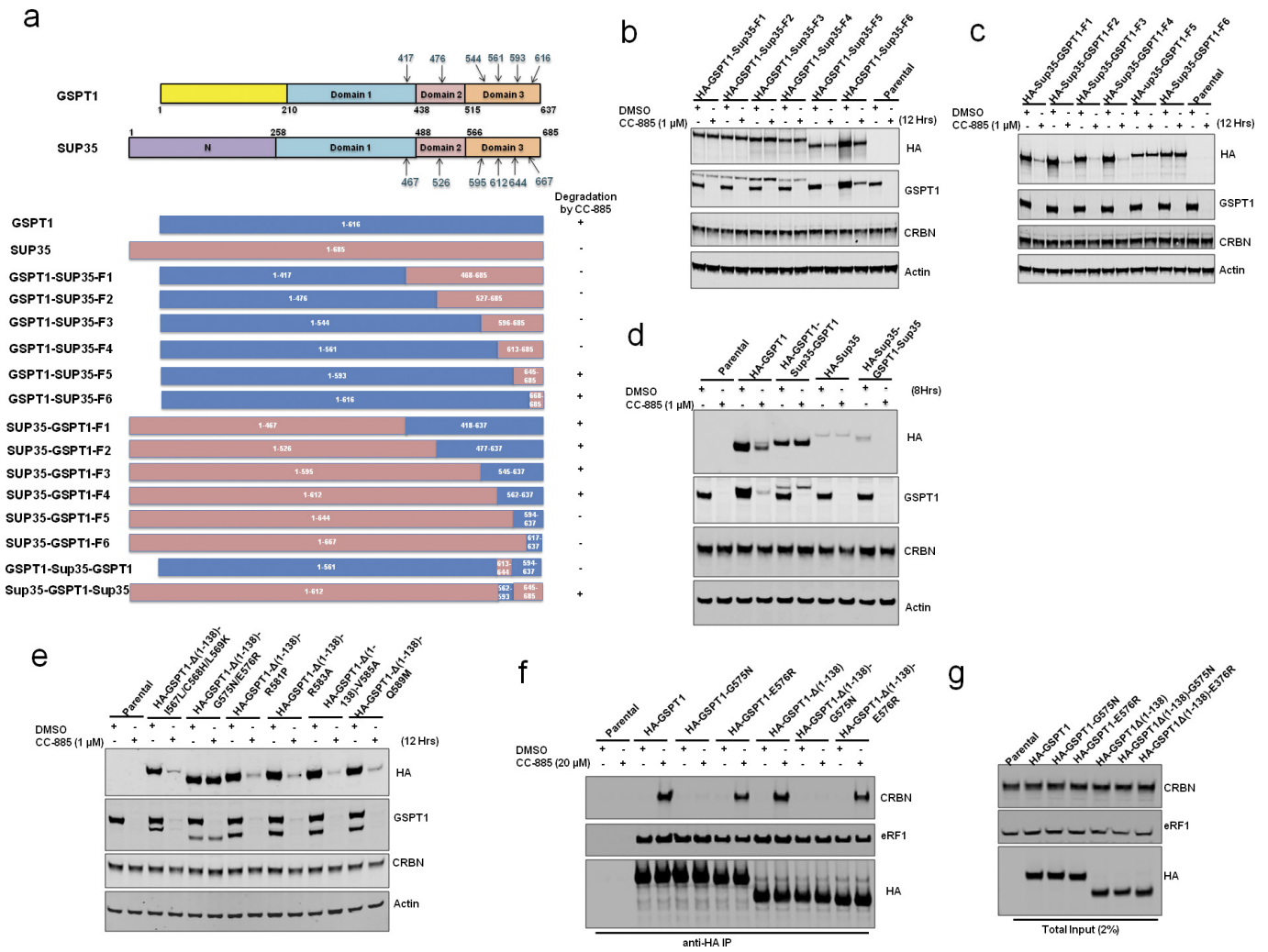

Extended Data Figure 5 | Identification of the region of GSPT1 indispensable for CC-885-dependent destruction. a, Schematic of human GSPT1 and *Saccharomyces cerevisiae* SUP35 chimaeras. Truncation analysis of GSPT1 revealed that domains 2 and 3 of GSPT1 contain the CC-885-dependent CRBN-binding motif (data not shown). In this region, GSPT1 and SUP35 share 53% sequence identity. Chimaeric fusion sites were selected from several stretches of identical regions to ensure proper folding of the resultant fusion product. Changes in protein level of these fusion proteins in 293T HEK cells in response to CC-885 treatment, as shown in **b–d**, is summarized on the right. +, protein degraded; −, no change of protein level. **b–d**, Immunoblot analysis of 293T HEK parental cells or cells stably expressing HA-tagged GSPT1, SUP35 or GSPT1–SUP35 chimaeric proteins. Note that SUP35 expression level is relatively low compared to GSPT1, possibly owing to its intrinsic instability when expressed in human cell lines. **e**, Immunoblot analysis of 293T HEK cells stably producing HA-tagged GSPT1 wild-type and variants. Non-conserved amino acids in GSPT1 as shown in Fig. 2a were replaced with corresponding residues in SUP35. **f**, **g**, Immunoblot analysis of anti-HA immunoprecipitates (**f**) and whole-cell extracts (**g**) of 293T HEK cells expressing GSPT1 wild-type and mutants. DMSO or CC-885 was added into the whole-cell extract after lysis for 6 h. For gel source data, see Supplementary Information Fig. 1.

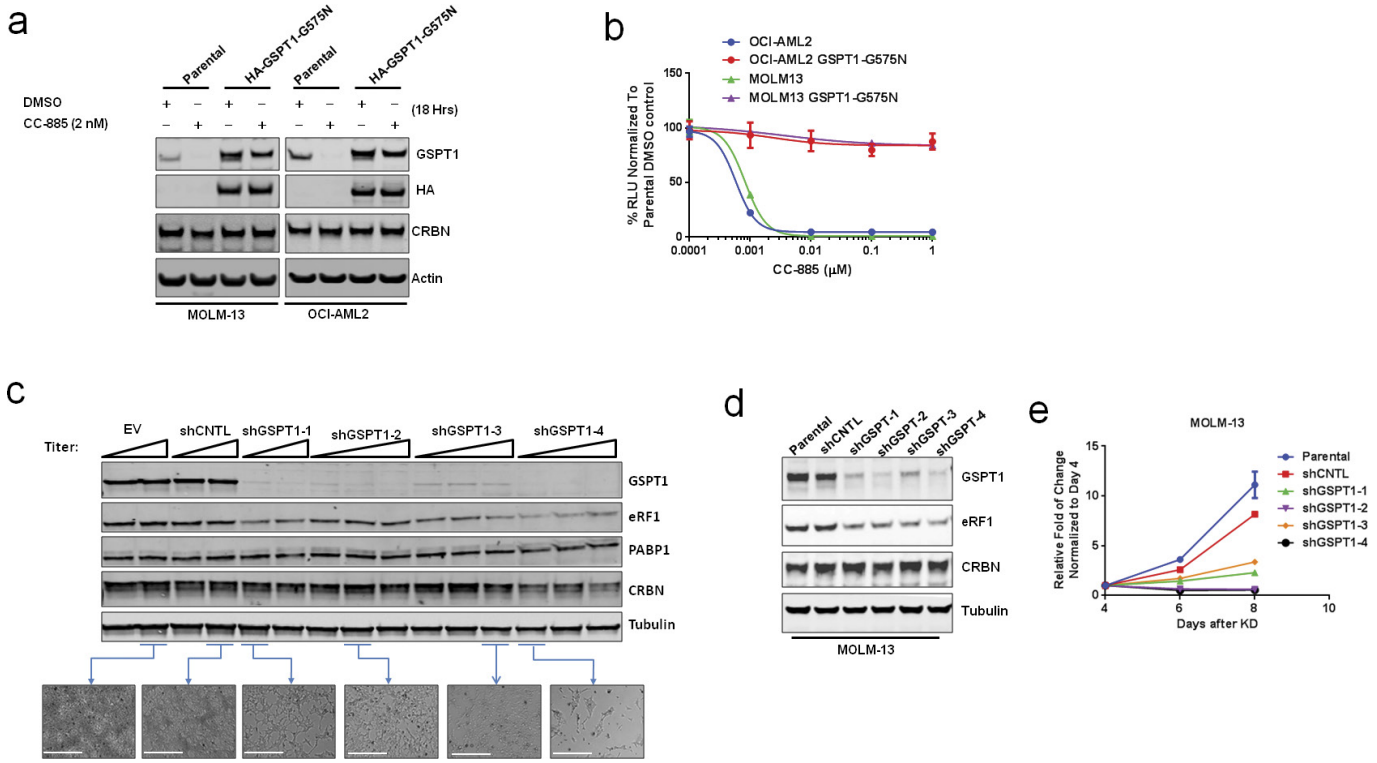

Extended Data Figure 6 | Loss of GSPT1 is the cause of growth inhibition induced by CC-885. a, Immunoblot analysis of MOLM-13 and OCI-AML2 parental cells or cells stably expressing HA-tagged GSPT1(G575N). Cells were treated with CC-885. **b**, Cells shown in **a** were incubated with CC-885 at the indicated concentration for 3 days. Cell proliferation was determined by CellTiter-Glo (CTG). Result is representative of three biological replicates. Data are presented as mean ± s.d., $n = 3$ technical replicates. **c**, 293T HEK cells were infected with an increased amount of empty lentiviral vector (EV) or vectors expressing control shRNA or any of the four GSPT1-specific shRNAs. Seven days after infection, cells were imaged using phase-contrast microscope (bottom) and collected for immunoblot analysis (top). Scale bars measure 0.5 mm. Images shown are representative of three captured images. **d**, **e**, Cell growth curve of MOLM-13 parental cells or cells transduced with lentiviral vectors expressing a control shRNA (shCNTL) or GSPT1 specific shRNA (shGSPT1-1 to 4). Immunoblot analyses of whole-cell extracts (**d**) were carried out at day 4 after transduction with lentiviral vectors. Cell growth (**e**) was quantified with CTG at day 4, 6, and 8 after transduction. Result is representative of three biological replicates. Data are mean ± s.d., $n = 3$ technical replicates. For gel source data, see Supplementary Information Fig. 1.

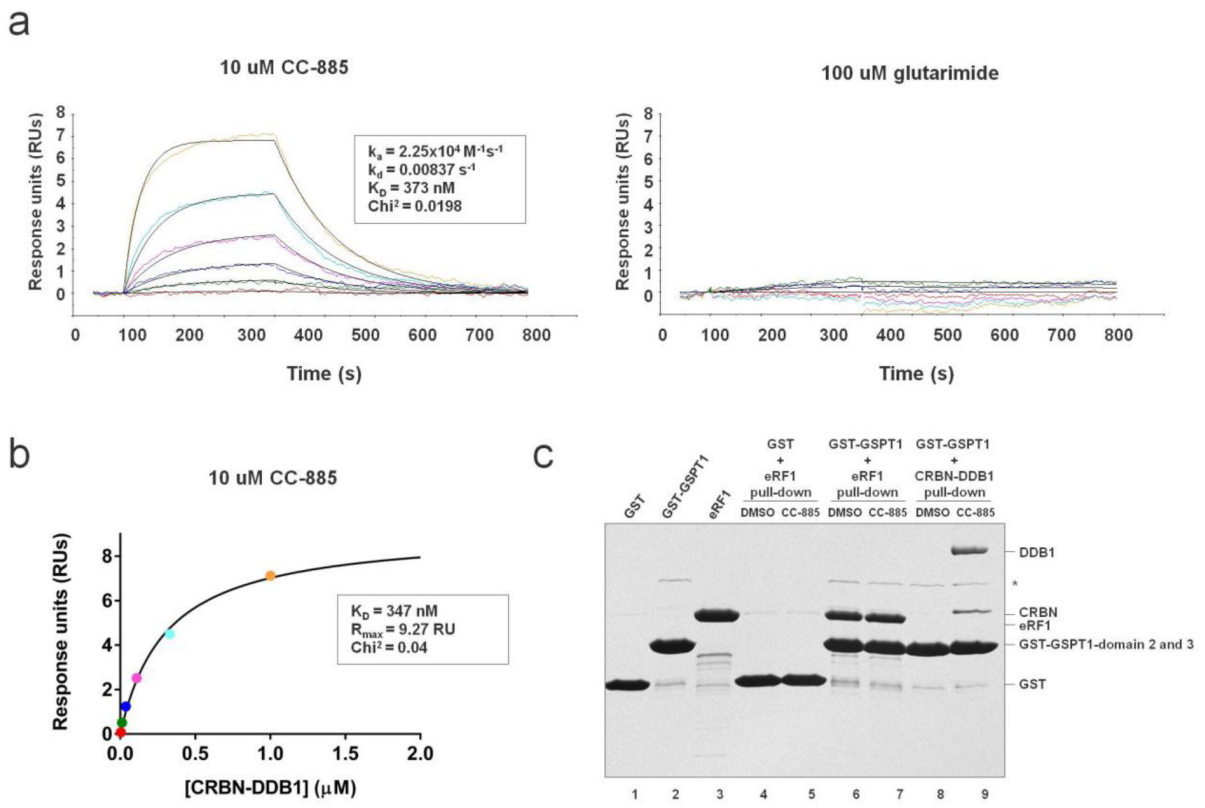

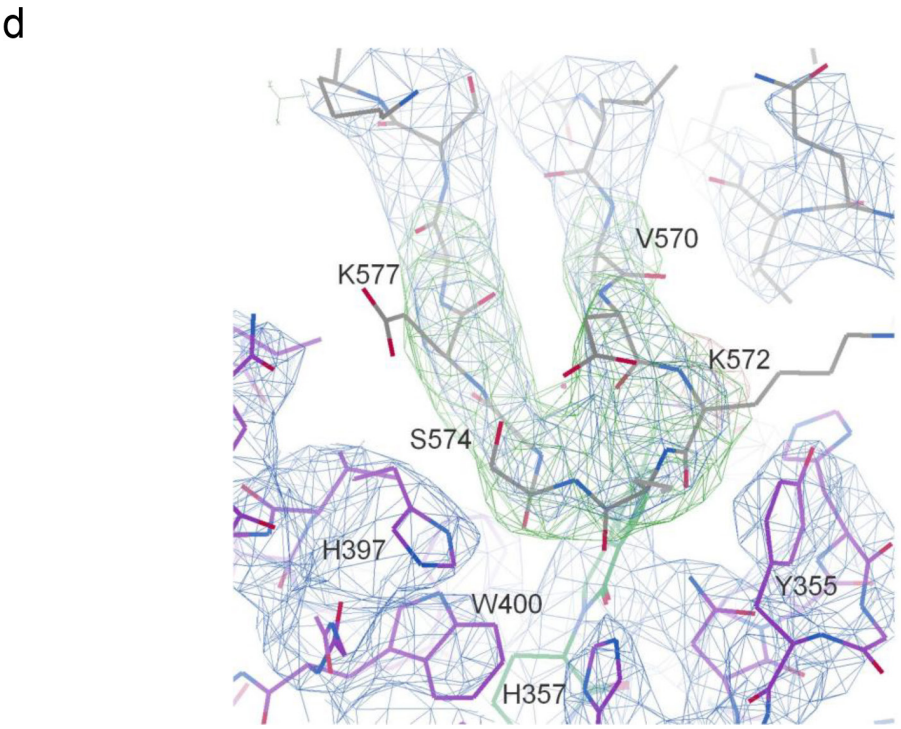

Extended Data Figure 7 | See next page for caption.

Extended Data Figure 7 | Kinetic parameters for cereblon–DDB1–CC-885 binding to GSPT1, and sample electron density from the crystal structure of the complex. a, Reference-corrected surface plasmon resonance binding curves for various concentrations of cereblon–DDB1 (threefold dilutions from 1 μM, coloured traces) flowed over a surface of covalently immobilized anti-GST antibody bound to GST–GSPT1 domains 2 and 3 at 10 °C in the presence of saturating levels of CC-885 or control compound glutarimide. Kinetic parameters shown were determined by fitting with a 1:1 kinetic binding model (black lines) using the Bioacore T200 kinetic analysis software package. Binding in the presence of gluatrimide could not be quantified. We show a representative set of curves from three independent experiments. For a 1:1 binding model where $A + B \leftrightarrows AB$, the net rate of complex formation is given by the equation $d[AB]/dt = k_a[A][B] - k_d[AB]$ and the rate of complex disassociation is given by $k_d[AB]$, where k_a is the association rate constant ($M^{-1}s^{-1}$) and k_d is the dissociation rate constant (s^{-1}). K_D, the equilibrium dissociation constant, is defined by $K_D = k_d/k_a$. R_{max} is a measurement of the analyte binding capacity, or maximum response. **b**, Analysis of the steady-state response versus the concentration of analyte in the presence of CC-885, and the determined affinity constant. **c**, GST–GSPT1 interacts with endogenous binding partner eRF1. We show that the purified GST–GSPT1 domains 2 and 3 (amino acids 437–633) protein used in this SPR binding assay and the electron miscroscopy experiments (Extended Data Fig. 8) is competent to bind purified eRF1 as reported in ref. 17. Coomassie stain, with lanes 1, 2 and 3 showing individual proteins. Lanes 4 and 5 show pull-down of GST; lanes 6 and 7 show pull-down of GST–GSPT1 domains 2 and 3, all were bound to magnetic glutathione beads incubated with eRF1 ± CC-885 for 1 h and washed three times. Lanes 8 and 9 show pull-down of GST-GSPT1 bound to magnetic glutathione beads incubated with CRBN–DDB1 ± CC-885 for 1 h and washed three times. This experiment was performed twice. For gel source data, see Supplementary Information Fig. 1. **d**, Sample electron density from the cereblon–DDB1–CC-885–GSPT1 crystal structure with cereblon residues shown in purple, GSPT1 residues shown in grey, and CC-885 shown in green. Refined $2F_o - F_c$ density is shown as a blue mesh contoured at 1.4σ. $F_o - F_c$ difference density, shown as a green mesh contoured at 4σ, was generated by a single round of Refmac5 refinement calculated in the absence of GSPT1 residues 570–577.

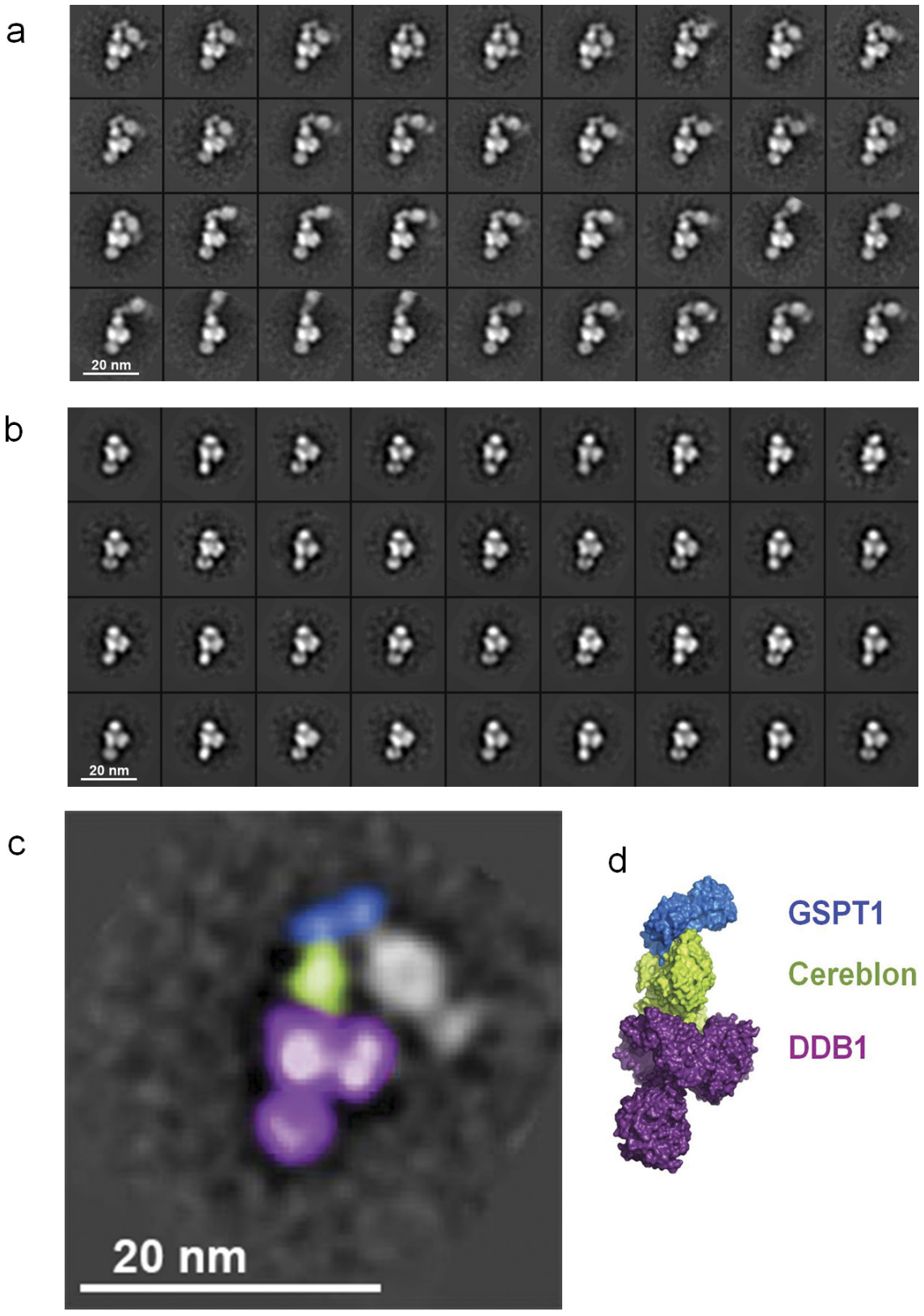

Extended Data Figure 8 | See next page for caption.

Extended Data Figure 8 | Imaging of GSPT1 binding to cereblon–DDB1–CC-885 by negative stain electron microscopy. a, Negative stain class averages of N-terminal-tagged GST–GSPT1 domain 2 and 3 (amino acids 437–633) bound to purified cereblon–DDB1 in the presence of CC-885. As the GST-tag was fused to the N terminus of domain 2 of GSPT1, domain 3 can be identified as mediating the interaction with cereblon. Whereas the GST tag appears flexible in position, the two domains of GSPT1 are consistent in their orientation with the cereblon–DDB1 complex. GST-dimerization mediates the binding of a second substrate in the majority of the classes. Each class average is composed of between 40 and 70 individual particles. This experiment was performed three times. **b**, Negative stain class averages of cereblon–DDB1 and GST–GSPT1 domains 2 and 3 (amino acids 437–633) in the presence of DMSO instead of CC-885. No classes containing bound substrate were observed in the absence of CC-885. Each class average is composed of between 40 and 70 individual particles. This experiment was performed once. **c**, A negative stain class average of GST–GSPT1 domains 2 and 3 bound to cereblon–DDB1–CC-885, with DDB1 shaded purple, cereblon shaded green, GSPT1 domains 2 and 3 shaded blue, and the second dimerized GST tag and second GSPT1 left uncoloured. **d**, For comparison, the crystal structure of GSPT1 domains 2 and 3 bound to cereblon–DDB1–CC-885 with DDB1 in purple, cereblon in green, and GSPT1 in blue. The electron micrographs revealed a consistent configuration of GSPT1 with cereblon in all complex class averages and confirmed that domain 3 mediates cereblon interactions on the basis of the orientation of the GST-tag.

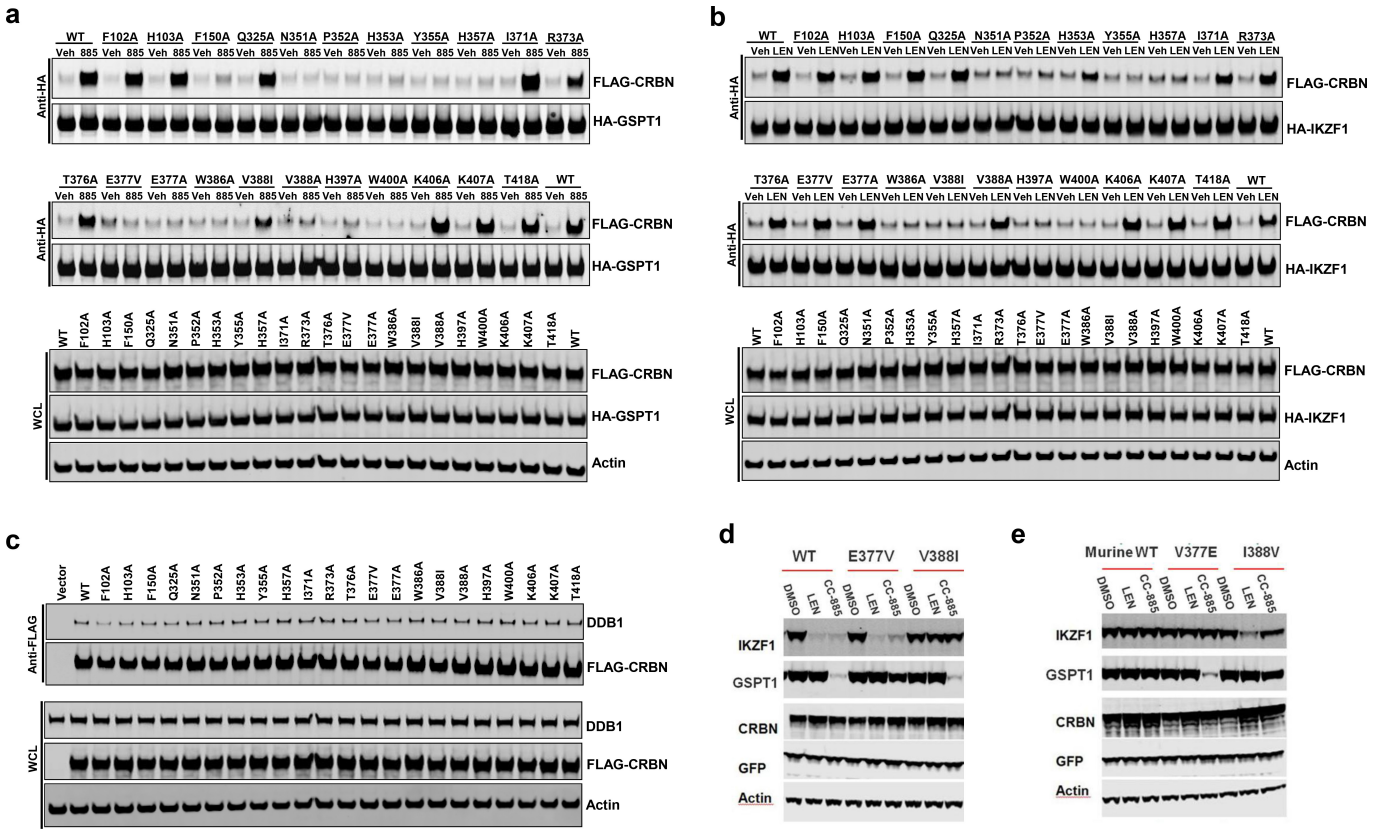

Extended Data Figure 9 | Effects of cereblon surface mutations on substrate binding. Cereblon and substrate proteins were co-expressed in 293FT *CRBN*$^{-/-}$ cells, co-immunoprecipitated in the presence or absence of CC-885 and lenalidomide, and analysed by western blot. **a**, Co-immunoprecipitation of GSPT1 with wild-type and mutant cereblon. veh, vehicle, DMSO; 885, 10 μM CC-885. **b**, Co-immunoprecipitation of Ikaros with wild-type and mutant cereblon. veh, vehicle, DMSO; LEN, 10 μM lenalidomide. **c**, Co-immunoprecipitation of DDB1 with wild-type and mutant cereblon. Results are representative of three biological replicates. **d**, **e**, Western blots showing the effect of lenalidomide or CC-885 on Ikaros and GSPT1 degradation; **d**, effect with human cereblon, **e**, effect with mouse cereblon. For convenience, the human amino acid numbering is used to discuss the corresponding residues in mouse. GFP and actin are shown as transfection and loading controls, respectively. This is a representative experiment of three biological replicates. For gel source data, see Supplementary Information Fig. 1.

Extended Data Table 1 | Data collection and refinement statistics from the cereblon–DDB1–CC-885–GSPT1 crystal structure

	CRBN-DDB1-CC-885-GSPT1
Data collection	
Space group	*P*2
Cell dimensions	
a, *b*, *c* (Å)	156.8 111.5 175.1
α, β, γ (°)	90 95.8 90
Resolution (Å)	50-3.6 (3.66-3.6)*
R_{merge} (%)	19.8 (79.6)
$I / \sigma I$	10.6 (2.1)
Completeness (%)	94.4 (93.9)
Redundancy	4.8 (4.5)
Refinement	
Resolution (Å)	50.0-3.6
No. reflections	62827
R_{work} / R_{free}	0.224 / 0.273
No. atoms	
Protein	25202
Ligand/ion	62/2
Water	0
B factors	
Protein	117.9
Ligand/ion	99.9/167.6
Water	N/A
r.m.s. deviations	
Bond lengths (Å)	0.017
Bond angles (°)	1.796

*Values in parentheses are for highest-resolution shell.